Bi-modulus materials consistent with a stored energy function: theory and numerical implementation

Marcos Latorre[a], Francisco J. Montáns[b,*]

[a] *Department of Biomedical Engineering*
Yale University, New Haven, CT, USA

[b] *Escuela Técnica Superior de Ingeniería Aeronáutica y del Espacio*
Universidad Politécnica de Madrid, Madrid, Spain

Abstract

Many materials present different behavior in tension and compression. Within the infinitesimal isotropic theory, the widely used approach based on the Ambartsumyan theory presents only three independent constants to preserve symmetry of the elasticity tensor. The reported finite element implementation of this and similar theories are complex and lack the convergence properties expected for a bi-linear material. In this work we address the problem through a hyperelastic approach, obtaining a simple and consistent framework which retain the four independent constants and yields the expected convergence characteristics of a bi-linear material. The Ambartsumyan model is obtained as a particular case within this framework.

Keywords: Bi-modulus materials, tension-compression asymmetry, finite elements, hyperelasticity, Ambartsumyan theory.

1. Introduction

The classical theory of infinitesimal isotropic elasticity considers only two independent material constants, for example the Young modulus E and the Poisson ratio ν; or alternatively, the bulk modulus K and the shear modulus (or the Lame constant) μ. However, many common materials present different elastic behavior in tension and in compression, for example different observed Young moduli, say E^+ in tension and E^- in compression.

*Corresponding author

Email addresses: marcos.latorre@yale.edu (Marcos Latorre), fco.montans@upm.es (Francisco J. Montáns)

Examples of these materials are concrete and ceramics [1], specially under damage [2], rocks [3, 4], graphite [5], nacre [6], polypropylene composites [7], asphalt-mixture materials [8], some cellular materials [9], Nitinol [10–12], etc. The resulting materials from 3D printing, may also show elastic tension-compression asymmetry [13]. Fibre-reinforced materials [14–16], biological tissues [17, 18] and cartilage [19], rubber [20], thin sheets (films) subject to local buckling [21, 22], and tensegrity structures as those used in space structures [23, 24] and cell mechanics [25], are also complex structures or materials which may be modelled using bimodulus materials. Table 1 gives some representative values of bimodulus materials. Therefore, for quite long time, attention has been placed in modelling this type of materials [14, 26], searching for a proper, consistent description of the theory [27], obtaining analytical solutions of beams [28] or plates [29, 30], including influence of bi-modularity in their stability [20, 22], and devising efficient implementations of that theory for finite element analyses [31]. In particular, many recent publications deal with the optimization of structures composed of bi-modulus materials and related inverse problems, see e.g. [32–36]. In these works, an important keystone is the constitutive algorithm for bi-modulus materials during the finite element simulations, where disappointing performance is reported.

Typically, the bi-modulus (bi-linear) materials are considered within the infinitesimal framework. Hence, in principle, they should present little additional difficulty to that of linear elasticity. However, according to the literature, the extension of the classical approach of elasticity to bi-modulus materials has proven to be challenging. A review of some of the theoretical approaches, as well as of the related difficulties in finite element implementations may be found in Sun et al [27]. One of the main issues in developing the theory is the definition of a bi-modulus material itself, in particular, which quantity produces the switch from "tension" to "compression" and, hence, which related moduli brings the material duality. The best-known theory for isotropic materials is that of Ambartsumyan [26], which proposed in a phenomenological manner that the switch should be controlled by the corresponding principal stress signs. A similar approach was followed by Medri for nonlinear hypoelasticity [37] and by Vijayakumar and Rao [38] for reinforced materials. In this case, the stress domain (longitudinal-transverse) was divided into eight zones, each one having its respective compliance matrix. The fiber reinforcement cases were also addressed by Jones [14] and Bert

[16]. They applied the Ambartsumyan model to these materials containing stress switches and introducing variations to improve consistency aspects in the theory; Jones by using a weighted compliance matrix and Bert by retaining a non-symmetric tangent. Indeed, an important issue in all these works is the symmetry of the constitutive matrix, so followers of the work of Ambartsumyan [26] frequently restrict the theory with the requirement (assumed implied from thermodynamic considerations) that $\nu^-/E^- = \nu^+/E^+$, where ν^+ and ν^- are the Poisson ratios for tension and compression respectively; see for instance the recent works [1, 31, 35, 36, 39, 40], among others. This leaves an "isotropic" theory restricted to only materials with three independent constants, a formulation criticised in [41] for arguably being incompatible with isotropy.

In addition to the mentioned restriction on the material constants, the finite element implementation of the bi-modulus isotropic materials has been cumbersome, and the numerical performance disappointing. Starting from the complex variational formulations [40] and their also complex associated finite element implementations [31], a relatively high number of iterations are needed to obtain a solution of a material which is conceptually just bi-linear; see for example the numerical implementations and the analyses performed in [35, 39, 42]. Indeed, in [42] it is inferred that the inconsistency of the Ambartsumyan model may be the reason why Newton convergence rates are slow. Smoothing techniques have been proposed to regularize the change of stiffness to improve convergence, e.g. [8, 36]. In structural optimization and inverse analyses, where the efficiency and robustness of the material algorithms are very important, the bi-modulus material is replaced by fictitious linear-elastic materials with properties of tension or compression depending on stored energy indices, see e.g. [32, 34], among others. However, we note that abrupt stiffness changes are present, for example, in finite element elastoplastic formulations, which are nowadays very efficient and preserve asymptotic quadratic convergence rates. In our opinion, a consistent theory and finite element implementation of bi-modulus materials should show, at least, similar performance.

Therefore, the purpose of this work is to present a consistent, hyperelasticity-based alternative for the problem addressed above which depends on *four* independent constants in the isotropic case, is more suitable for a direct and simpler implementation in a finite element

program and, furthermore, has an immediate extension to large strain isotropic hyperelasticity [43] (see below) and relatively simple for anisotropic materials as well [44]. We show by numerical examples that the efficiency is also as expected: only an additional iteration is needed from the linear case in homogeneous deformations. This iteration is needed when there is a transition from tension to compression during the loading procedure. In nonhomogeneous cases (where different stress points may change their state at different iterations), asymptotic second order convergence is attained. We also analyse the (non-algorithmic) reasons why some proposed alternatives may encounter difficulties in obtaining asymptotic quadratic convergence. Noteworthy, we show that the widely used Ambartsumyan model emerges as a very particular case within the present framework.

2. Hyperelastic materials exhibiting different behavior in tension and compression

A simple way to deal with a (hyper-)elastic isotropic material that shows a bi-linear mechanical response is to assume the existence of a strain energy function that depends on two bi-linear elastic constants.

2.1. Deviatoric-volumetric split of strains and stresses

Consider, for further use in bi-modulus formulations introduced below, the well-known decomposition of the infinitesimal strain tensor $\boldsymbol{\varepsilon}$ into deviatoric (distortional) $\boldsymbol{\varepsilon}^d$ and volumetric (dilatational) $\boldsymbol{\varepsilon}^v$ parts

$$\boldsymbol{\varepsilon} := \boldsymbol{\varepsilon}^d + \boldsymbol{\varepsilon}^v = (\boldsymbol{\varepsilon} - \boldsymbol{\varepsilon}^v) + \boldsymbol{\varepsilon}^v \tag{1}$$

$$= \left[\mathbb{I}^S - \frac{1}{3}(\mathbf{I}\otimes\mathbf{I})\right] : \boldsymbol{\varepsilon} + \frac{1}{3}(\mathbf{I}\otimes\mathbf{I}) : \boldsymbol{\varepsilon} \tag{2}$$

$$= \mathbb{P}^d : \boldsymbol{\varepsilon} + \mathbb{P}^v : \boldsymbol{\varepsilon} \tag{3}$$

where $(\mathbb{I}^S)_{ijkl} = \frac{1}{2}(\delta_{ik}\delta_{jl} + \delta_{il}\delta_{jk})$ is the fourth-order symmetric identity tensor written in terms of Kronecker's deltas, $\mathbb{P}^d$ is the fourth-order deviatoric projector tensor, $\mathbb{P}^v$ is the

fourth-order volumetric projector tensor, and we have used

$$\boldsymbol{\varepsilon}^v = \frac{1}{3}(\operatorname{tr}\boldsymbol{\varepsilon})\mathbf{I} = \frac{1}{3}\left(\boldsymbol{\varepsilon} : \mathbf{I}\right)\mathbf{I} = \frac{1}{3}\left(\mathbf{I}\otimes\mathbf{I}\right) : \boldsymbol{\varepsilon} \tag{4}$$

with $\mathbf{I}$ the second-order identity tensor. If we represent the local dilatation or volume strain as $e := \operatorname{tr}\boldsymbol{\varepsilon}$, then $\boldsymbol{\varepsilon}^v = \frac{1}{3}e\mathbf{I}$. Furthermore, deviatoric and volumetric strain tensors are independent (say uncoupled, "perpendicular") because

$$\boldsymbol{\varepsilon}^d : \boldsymbol{\varepsilon}^v = \boldsymbol{\varepsilon} : \boldsymbol{\varepsilon}^v - \boldsymbol{\varepsilon}^v : \boldsymbol{\varepsilon}^v = \frac{1}{3}(\operatorname{tr}\boldsymbol{\varepsilon})\left(\boldsymbol{\varepsilon} : \mathbf{I}\right) - \frac{1}{3}(\operatorname{tr}\boldsymbol{\varepsilon})\left(\boldsymbol{\varepsilon}^v : \mathbf{I}\right) = \frac{1}{3}(\operatorname{tr}\boldsymbol{\varepsilon})^2 - \frac{1}{3}(\operatorname{tr}\boldsymbol{\varepsilon})^2 = 0 \tag{5}$$

and also complementary by means of Eq. (1).

Similarly, the decomposition of the (kinematically infinitesimal) stress tensor $\boldsymbol{\sigma}$ into deviatoric (distortional) $\boldsymbol{\sigma}^d$ and volumetric (hydrostatic) $\boldsymbol{\sigma}^v$ parts reads

$$\boldsymbol{\sigma} := \boldsymbol{\sigma}^d + \boldsymbol{\sigma}^v = \mathbb{P}^d : \boldsymbol{\sigma} + \mathbb{P}^v : \boldsymbol{\sigma}$$

where $\boldsymbol{\sigma}^d : \boldsymbol{\sigma}^v = 0$. In this case, $p := \frac{1}{3}\operatorname{tr}\boldsymbol{\sigma}$ is the mean or hydrostatic stress[1] (or pressure) and $\boldsymbol{\sigma}^v = p\mathbf{I}$.

2.2. Strain-driven bi-modulus formulations

The strain energy function for a linear elastic isotropic material may be expressed in terms of any independent pair of elastic constants. For example, in terms of the shear $\mu = G$ and the bulk K *stiffness* moduli, it reads

$$\Psi\left(\boldsymbol{\varepsilon}\right) = \mu\boldsymbol{\varepsilon}^d : \boldsymbol{\varepsilon}^d + \frac{3}{2}K\boldsymbol{\varepsilon}^v : \boldsymbol{\varepsilon}^v = \mu\left\|\boldsymbol{\varepsilon}^d\right\|^2 + \frac{1}{2}Ke^2 =: \mathcal{W}(\boldsymbol{\varepsilon}^d) + \mathcal{U}(e) \tag{6}$$

where $\|\cdot\|$ is the usual 2-norm. The first addend $\mathcal{W}(\boldsymbol{\varepsilon}^d)$ accounts for the distortional stored energy and the second addend $\mathcal{U}(e)$ for the dilatational one, which, importantly, may change

[1] p may alternatively be defined to be positive in compression and negative in tension, but we do not use such convention here.

independent to each other. In principal strain (and stress) directions, we can write

$$\Psi\left(\boldsymbol{\varepsilon}\right)=\mathcal{W}(\boldsymbol{\varepsilon}^{d})+\mathcal{U}(e)=\mu\varepsilon_{1}^{d2}+\mu\varepsilon_{2}^{d2}+\mu\varepsilon_{3}^{d2}+\frac{1}{2}Ke^{2} \tag{7}$$

where we use $\varepsilon^{d2}=(\varepsilon^{d})^{2}$. The stresses $\boldsymbol{\sigma}=d\Psi\left(\boldsymbol{\varepsilon}\right)/d\boldsymbol{\varepsilon}$ that directly derive from Eq. (6) are

$$\boldsymbol{\sigma}=\frac{d\mathcal{W}(\boldsymbol{\varepsilon}^{d})}{d\boldsymbol{\varepsilon}^{d}}:\frac{d\boldsymbol{\varepsilon}^{d}}{d\boldsymbol{\varepsilon}}+\frac{d\mathcal{U}(e)}{de}\frac{de}{d\boldsymbol{\varepsilon}}=2\mu\boldsymbol{\varepsilon}^{d}:\mathbb{P}^{d}+Ke\mathbf{I}=2\mu\boldsymbol{\varepsilon}^{d}+3K\boldsymbol{\varepsilon}^{v}=\boldsymbol{\sigma}^{d}+\boldsymbol{\sigma}^{v} \tag{8}$$

where we used $\boldsymbol{\varepsilon}^{d}:\mathbb{P}^{d}=\boldsymbol{\varepsilon}^{d}$, hence $\boldsymbol{\sigma}^{d}=2\mu\boldsymbol{\varepsilon}^{d}$ and $\boldsymbol{\sigma}^{v}=3K\boldsymbol{\varepsilon}^{v}$, the latter also yielding $p=Ke$ in scalar form.

A coupled form of the strain energy function is obtained by introducing $\boldsymbol{\varepsilon}^{d}=\boldsymbol{\varepsilon}-\boldsymbol{\varepsilon}^{v}$, from Eq. (1), into Eq. (6)

$$\Psi\left(\boldsymbol{\varepsilon}\right)=\mu\boldsymbol{\varepsilon}:\boldsymbol{\varepsilon}+\left(\frac{3}{2}K-\mu\right)\boldsymbol{\varepsilon}^{v}:\boldsymbol{\varepsilon}^{v}=\mu\left\|\boldsymbol{\varepsilon}\right\|^{2}+\frac{1}{2}\lambda e^{2} \tag{9}$$

which is now expressed in terms of the first ($\lambda=K-\frac{2}{3}\mu$) and second (μ) Lamé *stiffness* moduli. In principal strain (and stress) directions

$$\Psi\left(\boldsymbol{\varepsilon}\right)=\mu\varepsilon_{1}^{2}+\mu\varepsilon_{2}^{2}+\mu\varepsilon_{3}^{2}+\frac{1}{2}\lambda e^{2} \tag{10}$$

The stresses that directly derive from Eq. (9) are

$$\boldsymbol{\sigma}=\frac{d\Psi\left(\boldsymbol{\varepsilon}\right)}{d\boldsymbol{\varepsilon}}=2\mu\boldsymbol{\varepsilon}+\lambda e\mathbf{I}=\boldsymbol{\sigma}^{d}+\boldsymbol{\sigma}^{v} \tag{11}$$

where, in general, $\boldsymbol{\sigma}^{d}\neq2\mu\boldsymbol{\varepsilon}$ or $\boldsymbol{\sigma}^{v}\neq\lambda e\mathbf{I}$, but $\boldsymbol{\sigma}^{d}=2\mu(\boldsymbol{\varepsilon}-\frac{1}{3}e\boldsymbol{I})$ and $\boldsymbol{\sigma}^{v}=(\lambda+\frac{2}{3}\mu)e\boldsymbol{I}$.

2.2.1. Uncoupled strain-driven bi-modulus formulation

Noticing the special fact that each term on the right-hand side in Eq. (7) is expressed in terms of a single elastic constant and a single strain component, a bi-linear generalization is straightforward using a deviatoric-strain-driven shear *stiffness* bi-modulus in each one of

the first three addends

$$\hat{\mu}_i = \left\{ \begin{array}{lll} \hat{\mu}^+ & \text{if} & \varepsilon_i^d \geq 0 \\ \hat{\mu}^- & \text{if} & \varepsilon_i^d < 0 \end{array} \right\} \ , \quad i = 1, 2, 3 \tag{12}$$

and a volumetric-strain-driven bulk *stiffness* bi-modulus

$$\hat{K} = \left\{ \begin{array}{lll} \hat{K}^+ & \text{if} & e \geq 0 \\ \hat{K}^- & \text{if} & e < 0 \end{array} \right. \tag{13}$$

Note that, in this case, deviatoric and volumetric strain switches control respective effective values for $\hat{\mu}_i$ and $\hat{K}$ independent to each other. Hence, the resulting strain energy function for uncoupled strain-driven bi-linear elastic isotropic materials

$$\hat{\Psi}\left(\boldsymbol{\varepsilon}\right) = \hat{\mathcal{W}}(\boldsymbol{\varepsilon}^d) + \hat{\mathcal{U}}(e) = \hat{\mu}_1 \varepsilon_1^{d2} + \hat{\mu}_2 \varepsilon_2^{d2} + \hat{\mu}_3 \varepsilon_3^{d2} + \tfrac{1}{2}\hat{K} e^2 \tag{14}$$

is uncoupled in terms of deviatoric and volumetric strain contributions and depends on *four* independent material constants overall.

2.2.2. Coupled strain-driven bi-modulus formulation

Each term on the right-hand side in Eq. (10) is also expressed in terms of a single elastic constant and strain component. Hence, a bi-linear generalization is also possible, in this case using a total-strain-driven shear *stiffness* bi-modulus in each one of the first three addends

$$\bar{\mu}_i = \left\{ \begin{array}{lll} \bar{\mu}^+ & \text{if} & \varepsilon_i \geq 0 \\ \bar{\mu}^- & \text{if} & \varepsilon_i < 0 \end{array} \right\} \ , \quad i = 1, 2, 3 \tag{15}$$

and a volumetric-strain-driven Lamé *stiffness* bi-modulus

$$\bar{\lambda} = \left\{ \begin{array}{lll} \bar{\lambda}^+ & \text{if} & e \geq 0 \\ \bar{\lambda}^- & \text{if} & e < 0 \end{array} \right. \tag{16}$$

Since total and volumetric strain switches are not independent to each other, that is, a change in sign of e may imply a change in sign of ε_i, note that $\bar{\mu}^+$ and $\bar{\mu}^-$ are, in general,

different from $\hat{\mu}^+$ and $\hat{\mu}^-$. Nevertheless, the resulting strain energy function for coupled strain-driven bi-linear elastic isotropic materials

$$\bar{\Psi}\left(\boldsymbol{\varepsilon}\right) = \bar{\mu}_1 \varepsilon_1^{d2} + \bar{\mu}_2 \varepsilon_2^{d2} + \bar{\mu}_3 \varepsilon_3^{d2} + \tfrac{1}{2}\bar{\lambda} e^2 \tag{17}$$

still depends on *four* independent material constants overall.

2.3. Stress-driven bi-modulus formulations

Following the Legendre transformation $\Psi^c(\boldsymbol{\sigma}) = \boldsymbol{\sigma} : \boldsymbol{\varepsilon} - \Psi(\boldsymbol{\varepsilon})$ we define $\Psi^c\left(\boldsymbol{\sigma}\right)$ as the complementary strain energy function to $\Psi\left(\boldsymbol{\varepsilon}\right)$, which for a linear elastic isotropic material can be obtained through the replacement $\Psi^c\left(\boldsymbol{\sigma}\right) = \Psi\left(\boldsymbol{\varepsilon}(\boldsymbol{\sigma})\right)$. If $\Psi\left(\boldsymbol{\varepsilon}\right)$ is uncoupled, as in Eq. (6), then $\Psi^c(\boldsymbol{\sigma}) = \mathcal{W}(\boldsymbol{\varepsilon}^d(\boldsymbol{\sigma}^d)) + \mathcal{U}(\boldsymbol{\varepsilon}^v(\boldsymbol{\sigma}^v))$, which, with $\boldsymbol{\varepsilon}^d(\boldsymbol{\sigma}^d) = \frac{1}{2\mu}\boldsymbol{\sigma}^d$ and $\boldsymbol{\varepsilon}^v(\boldsymbol{\sigma}^v) = \frac{1}{3K}\boldsymbol{\sigma}^v$, reads

$$\Psi^c(\boldsymbol{\sigma}) = \frac{1}{4\mu}\boldsymbol{\sigma}^d : \boldsymbol{\sigma}^d + \frac{1}{6K}\boldsymbol{\sigma}^v : \boldsymbol{\sigma}^v = \frac{1}{4\mu}\left\|\boldsymbol{\sigma}^d\right\|^2 + \frac{1}{2K}p^2 := \mathcal{W}^c(\boldsymbol{\sigma}^d) + \mathcal{U}^c(p) \tag{18}$$

which is expressed in terms of the shear $1/\mu$ and bulk $1/K$ *compliance* (or *flexibility*) moduli. In principal stress (and strain) directions

$$\Psi^c(\boldsymbol{\sigma}) = \mathcal{W}^c(\boldsymbol{\sigma}^d) + \mathcal{U}^c(p) = \frac{1}{4\mu}\sigma_1^{d2} + \frac{1}{4\mu}\sigma_2^{d2} + \frac{1}{4\mu}\sigma_3^{d2} + \frac{1}{2K}p^2 \tag{19}$$

The strains $\boldsymbol{\varepsilon} = d\Psi^c\left(\boldsymbol{\sigma}\right)/d\boldsymbol{\sigma}$ that directly derive from Eq. (18) are

$$\boldsymbol{\varepsilon} = \frac{d\mathcal{W}^c(\boldsymbol{\sigma}^d)}{d\boldsymbol{\sigma}^d} : \frac{d\boldsymbol{\sigma}^d}{d\boldsymbol{\sigma}} + \frac{d\mathcal{U}^c(p)}{dp}\frac{dp}{d\boldsymbol{\sigma}} = \frac{1}{2\mu}\boldsymbol{\sigma}^d : \mathbb{P}^d + \frac{p}{3K}\mathbf{I} = \frac{1}{2\mu}\boldsymbol{\sigma}^d + \frac{1}{3K}\boldsymbol{\sigma}^v = \boldsymbol{\varepsilon}^d + \boldsymbol{\varepsilon}^v \tag{20}$$

where $\boldsymbol{\sigma}^d : \mathbb{P}^d = \boldsymbol{\sigma}^d$, and one recovers $\boldsymbol{\varepsilon}^d = \frac{1}{2\mu}\boldsymbol{\sigma}^d$ and $\boldsymbol{\varepsilon}^v = \frac{1}{3K}\boldsymbol{\sigma}^v$, or $e = \frac{p}{K}$.

A coupled form of the complementary strain energy function is obtained by introducing $\boldsymbol{\sigma}^d = \boldsymbol{\sigma} - \boldsymbol{\sigma}^v$ into Eq. (18)

$$\Psi^c(\boldsymbol{\sigma}) = \frac{1}{4\mu}\boldsymbol{\sigma} : \boldsymbol{\sigma} + \left(\frac{1}{6K} - \frac{1}{4\mu}\right)\boldsymbol{\sigma}^v : \boldsymbol{\sigma}^v = \frac{1}{4\mu}\left\|\boldsymbol{\sigma}\right\|^2 - \frac{9}{2\zeta}p^2 \tag{21}$$

which is expressed in terms of the herein called first ($\frac{1}{\zeta} = \frac{1}{6\mu} - \frac{1}{9K}$) and second ($\frac{1}{\mu}$) Lamé

compliance moduli (by obvious comparison to Eq. (9)). Note that ζ has been defined such that $\zeta > 0$ if $3K > 2\mu > 0$, which also yields $\lambda > 0$, and that $\zeta = 9((\frac{2}{3}\mu)^{-1} - K^{-1})^{-1} \neq K - \frac{2}{3}\mu = \lambda$. In fact, $\zeta = (18\mu K)/(3K - 2\mu) = E/\nu$, with E the Young modulus and ν the Poisson ratio for linear elastic materials. In principal stress (and strain) directions

$$\Psi^c(\boldsymbol{\sigma}) = \frac{1}{4\mu}\sigma_1^2 + \frac{1}{4\mu}\sigma_2^2 + \frac{1}{4\mu}\sigma_3^2 - \frac{9}{2\zeta}p^2 \tag{22}$$

The strains that directly derive from Eq. (21) are

$$\boldsymbol{\varepsilon} = \frac{d\Psi^c(\boldsymbol{\sigma})}{d\boldsymbol{\sigma}} = \frac{1}{2\mu}\boldsymbol{\sigma} - \frac{1}{\zeta}3p\mathbf{I} = \boldsymbol{\varepsilon}^d + \boldsymbol{\varepsilon}^v \tag{23}$$

where $\boldsymbol{\varepsilon}^d \neq \frac{1}{2\mu}\boldsymbol{\sigma}$ or $\boldsymbol{\varepsilon}^v \neq -\frac{3}{\zeta}p\mathbf{I}$, in general. Hooke's law is immediately recovered for $\zeta = E/\nu$ and $2\mu = E/(1+\nu)$

$$\boldsymbol{\varepsilon} = \frac{1+\nu}{E}\boldsymbol{\sigma} - \frac{\nu}{E}(\operatorname{tr}\boldsymbol{\sigma})\mathbf{I} \tag{24}$$

2.3.1. Uncoupled stress-driven bi-modulus formulation

Similarly to our motivation to posit strain-driven formulations above, each term on the right-hand side in Eq. (19) is expressed in terms of a single elastic constant and stress component. Hence, a bi-linear generalization follows by using a deviatoric-stress-driven shear *compliance* bi-modulus in each one of the first three addends

$$\frac{1}{\tilde{\mu}_i} = \left\{ \begin{array}{ll} \dfrac{1}{\tilde{\mu}^+} & \text{if} \quad \sigma_i^d \geq 0 \\ \dfrac{1}{\tilde{\mu}^-} & \text{if} \quad \sigma_i^d < 0 \end{array} \right\}, \quad i = 1,2,3 \tag{25}$$

and a volumetric-stress-driven *compliance* bulk bi-modulus

$$\frac{1}{\tilde{K}} = \left\{ \begin{array}{ll} \dfrac{1}{\tilde{K}^+} & \text{if} \quad p \geq 0 \\ \dfrac{1}{\tilde{K}^-} & \text{if} \quad p < 0 \end{array} \right. \tag{26}$$

Again in this case, deviatoric and volumetric stress switches control respective effective values for $\tilde{\mu}_i$ and $\tilde{K}$ independent to each other. Hence, the resulting complementary strain energy

function for uncoupled stress-driven bi-linear elastic isotropic materials

$$\tilde{\Psi}^c(\boldsymbol{\sigma}) = \tilde{\mathcal{W}}^c(\boldsymbol{\sigma}^d) + \tilde{\mathcal{U}}^c(p) = \frac{1}{4\tilde{\mu}_1}\sigma_1^{d2} + \frac{1}{4\tilde{\mu}_2}\sigma_2^{d2} + \frac{1}{4\tilde{\mu}_3}\sigma_3^{d2} + \frac{1}{2\tilde{K}}p^2 \tag{27}$$

is uncoupled in terms of deviatoric and volumetric stress contributions and depends on *four* independent material constants overall.

2.3.2. Coupled stress-driven bi-modulus formulation

Eq. (22), also expressed in terms of respective single elastic constants and stress components, motivates a possible bi-linear generalization, in this case using a total-stress-driven shear *compliance* bi-modulus in each one of the first three addends

$$\frac{1}{\check{\mu}_i} = \left\{ \begin{array}{ll} \dfrac{1}{\check{\mu}^+} & \text{if} \quad \sigma_i \geq 0 \\ \dfrac{1}{\check{\mu}^-} & \text{if} \quad \sigma_i < 0 \end{array} \right\} , \quad i = 1, 2, 3 \tag{28}$$

and a volumetric-stress-driven Lamé *compliance* bi-modulus

$$\frac{1}{\check{\zeta}} = \left\{ \begin{array}{ll} \dfrac{1}{\check{\zeta}^+} & \text{if} \quad p \geq 0 \\ \dfrac{1}{\check{\zeta}^-} & \text{if} \quad p < 0 \end{array} \right. \tag{29}$$

Since total and volumetric stress switches are not independent to each other, that is, a change in sign of p may imply a change in sign of σ_i, then $\tilde{\mu}^+$ and $\tilde{\mu}^-$ are, in general, different from $\check{\mu}^+$ and $\check{\mu}^-$. The resulting complementary strain energy function for coupled stress-driven bi-linear elastic isotropic materials

$$\check{\Psi}^c(\boldsymbol{\sigma}) = \frac{1}{4\check{\mu}_1}\sigma_1^2 + \frac{1}{4\check{\mu}_2}\sigma_2^2 + \frac{1}{4\check{\mu}_3}\sigma_3^2 - \frac{9}{2\check{\zeta}}p^2 \tag{30}$$

still depends on *four* independent material constants overall.

2.4. Stresses and tangent stiffness moduli for strain-driven formulations

2.4.1. Uncoupled strain-driven bi-modulus formulation

The stresses that directly derive from Eq. (14) are

$$\boldsymbol{\sigma} = \frac{d\hat{\Psi}\left(\boldsymbol{\varepsilon}\right)}{d\boldsymbol{\varepsilon}} = \frac{d\hat{\mathcal{W}}(\boldsymbol{\varepsilon}^d)}{d\boldsymbol{\varepsilon}^d} : \frac{d\boldsymbol{\varepsilon}^d}{d\boldsymbol{\varepsilon}} + \frac{d\hat{\mathcal{U}}(e)}{de}\frac{de}{d\boldsymbol{\varepsilon}} = \frac{d\hat{\mathcal{W}}(\boldsymbol{\varepsilon}^d)}{d\boldsymbol{\varepsilon}^d} : \mathbb{P}^d + \frac{d\hat{\mathcal{U}}(e)}{de}\mathbf{I} \tag{31}$$

where both the fictitious (non-deviatoric, in general) stresses $d\hat{\mathcal{W}}(\boldsymbol{\varepsilon}^d)/d\boldsymbol{\varepsilon}^d$, expressed in terms of the principal basis vectors $\mathbf{N}_i$, and $d\hat{\mathcal{U}}(e)/de$ are

$$\frac{d\hat{\mathcal{W}}(\boldsymbol{\varepsilon}^d)}{d\boldsymbol{\varepsilon}^d} = \sum_{i=1}^{3} 2\hat{\mu}_i\varepsilon_i^d\mathbf{N}_i \otimes \mathbf{N}_i \quad \text{and} \quad \frac{d\hat{\mathcal{U}}(e)}{de} = \hat{K}e \tag{32}$$

The *exact* and *symmetric* tangent stiffness tensor is

$$\mathbb{C} = \frac{d\boldsymbol{\sigma}}{d\boldsymbol{\varepsilon}} = \frac{d^2\hat{\Psi}\left(\boldsymbol{\varepsilon}\right)}{d\boldsymbol{\varepsilon} \otimes d\boldsymbol{\varepsilon}} = \mathbb{P}^d : \frac{d^2\hat{\mathcal{W}}(\boldsymbol{\varepsilon}^d)}{d\boldsymbol{\varepsilon}^d \otimes d\boldsymbol{\varepsilon}^d} : \mathbb{P}^d + \frac{d^2\hat{\mathcal{U}}(e)}{de^2}\mathbf{I} \otimes \mathbf{I} \tag{33}$$

where $d^2\hat{\mathcal{U}}(e)/de^2 = \hat{K}$ and the fourth-order tensor $d^2\hat{\mathcal{W}}(\boldsymbol{\varepsilon}^d)/d\boldsymbol{\varepsilon}^d \otimes d\boldsymbol{\varepsilon}^d$ reads [45]

$$\frac{d^2\hat{\mathcal{W}}(\boldsymbol{\varepsilon}^d)}{d\boldsymbol{\varepsilon}^d \otimes d\boldsymbol{\varepsilon}^d} = \sum_{i=1}^{3} 2\hat{\mu}_i\mathbb{N}_{iiii} + \sum_{i=1}^{3}\sum_{j\neq i} \frac{2\hat{\mu}_j\varepsilon_j^d - 2\hat{\mu}_i\varepsilon_i^d}{\varepsilon_j^d - \varepsilon_i^d}\frac{1}{2}\left(\mathbb{N}_{ijij} + \mathbb{N}_{ijji}\right) \tag{34}$$

with

$$\mathbb{N}_{ijkl} := \mathbf{N}_i \otimes \mathbf{N}_j \otimes \mathbf{N}_k \otimes \mathbf{N}_l \tag{35}$$

Note that the shear components of $\mathbb{C}$ in the basis of principal directions, obtained from Eq. (34), depend on relative values of principal deviatoric strains ε_i^d and ε_j^d, $i = 1, 2, 3$, $i \neq j$, particularly when $\text{sign}[\varepsilon_i^d] \neq \text{sign}[\varepsilon_j^d]$, because then $\hat{\mu}_i \neq \hat{\mu}_j$ (say $\mu^+ \neq \mu^-$). In contrast, if $\text{sign}[\varepsilon_i^d] = \text{sign}[\varepsilon_j^d]$, then $\hat{\mu}_i = \hat{\mu}_j$ ($= \mu^+$, say) and the component $(\hat{\mu}_j\varepsilon_j^d - \hat{\mu}_i\varepsilon_i^d)/(\varepsilon_j^d - \varepsilon_i^d)$ particularizes to $\hat{\mu}_i = \hat{\mu}_j$ ($= \mu^+$) in the principal plane ij.

2.4.2. Coupled strain-driven bi-modulus formulation

The stresses that derive from Eq. (17) are

$$\boldsymbol{\sigma} = \frac{d\bar{\Psi}(\boldsymbol{\varepsilon})}{d\boldsymbol{\varepsilon}} = \sum_{i=1}^{3} 2\bar{\mu}_i \varepsilon_i \mathbf{N}_i \otimes \mathbf{N}_i + \bar{\lambda} e \mathbf{I} \tag{36}$$

The *exact* and *symmetric* tangent stiffness tensor is

$$\mathbb{C} = \frac{d^2\bar{\Psi}(\boldsymbol{\varepsilon})}{d\boldsymbol{\varepsilon} \otimes d\boldsymbol{\varepsilon}} = \sum_{i=1}^{3} 2\bar{\mu}_i \mathbb{N}_{iiii} + \sum_{i=1}^{3} \sum_{j \neq i} \frac{2\bar{\mu}_j \varepsilon_j - 2\bar{\mu}_i \varepsilon_i}{\varepsilon_j - \varepsilon_i} \frac{1}{2} \left(\mathbb{N}_{ijij} + \mathbb{N}_{ijji} \right) + \bar{\lambda} \mathbf{I} \otimes \mathbf{I} \tag{37}$$

2.5. Strains and tangent compliance moduli for stress-driven formulations

2.5.1. Uncoupled stress-driven bi-modulus formulation

The strains that directly derive from Eq. (27) are

$$\boldsymbol{\varepsilon} = \frac{d\tilde{\Psi}^c(\boldsymbol{\sigma})}{d\boldsymbol{\sigma}} = \frac{d\tilde{\mathcal{W}}^c(\boldsymbol{\sigma}^d)}{d\boldsymbol{\sigma}^d} : \frac{d\boldsymbol{\sigma}^d}{d\boldsymbol{\sigma}} + \frac{d\tilde{\mathcal{U}}^c(p)}{dp} \frac{dp}{d\boldsymbol{\sigma}} = \frac{d\tilde{\mathcal{W}}^c(\boldsymbol{\sigma}^d)}{d\boldsymbol{\sigma}^d} : \mathbb{P}^d + \frac{1}{3} \frac{d\tilde{\mathcal{U}}^c(p)}{dp} \mathbf{I} \tag{38}$$

where both the fictitious (non-deviatoric, in general) strains $d\tilde{\mathcal{W}}^c(\boldsymbol{\sigma}^d)/d\boldsymbol{\varepsilon}^d$, expressed in terms of the principal basis vectors $\mathbf{N}_i$, and $d\hat{\mathcal{U}}^c(p)/dp$ are

$$\frac{d\tilde{\mathcal{W}}^c(\boldsymbol{\sigma}^d)}{d\boldsymbol{\sigma}^d} = \sum_{i=1}^{3} \frac{1}{2\tilde{\mu}_i} \sigma_i^d \mathbf{N}_i \otimes \mathbf{N}_i \quad \text{and} \quad \frac{d\tilde{\mathcal{U}}^c(p)}{dp} = \frac{p}{\tilde{K}} \tag{39}$$

The *exact* and *symmetric* tangent compliance tensor is

$$\mathbb{S} = \frac{d\boldsymbol{\varepsilon}}{d\boldsymbol{\sigma}} = \frac{d^2\tilde{\Psi}^c(\boldsymbol{\sigma})}{d\boldsymbol{\sigma} \otimes d\boldsymbol{\sigma}} = \mathbb{P}^d : \frac{d^2\tilde{\mathcal{W}}^c(\boldsymbol{\sigma}^d)}{d\boldsymbol{\sigma}^d \otimes d\boldsymbol{\sigma}^d} : \mathbb{P}^d + \frac{1}{9} \frac{d^2\tilde{\mathcal{U}}^c(p)}{dp^2} \mathbf{I} \otimes \mathbf{I} \tag{40}$$

where $d^2\tilde{\mathcal{U}}^c(p)/dp^2 = 1/\tilde{K}$ and the fourth-order tensor $d^2\mathcal{W}^c(\boldsymbol{\sigma}^d)/d\boldsymbol{\sigma}^d \otimes d\boldsymbol{\sigma}^d$ reads

$$\frac{d^2\tilde{\mathcal{W}}^c(\boldsymbol{\sigma}^d)}{d\boldsymbol{\sigma}^d \otimes d\boldsymbol{\sigma}^d} = \sum_{i=1}^{3} \frac{1}{2\tilde{\mu}_i} \mathbb{N}_{iiii} + \sum_{i=1}^{3} \sum_{j \neq i} \frac{\frac{1}{2\tilde{\mu}_j} \sigma_j^d - \frac{1}{2\tilde{\mu}_i} \sigma_i^d}{\sigma_j^d - \sigma_i^d} \frac{1}{2} \left(\mathbb{N}_{ijij} + \mathbb{N}_{ijji} \right) \tag{41}$$

2.5.2. Coupled stress-driven bi-modulus formulation

The strains that derive from Eq. (30) are

$$\boldsymbol{\varepsilon} = \frac{d\breve{\Psi}^c(\boldsymbol{\sigma})}{d\boldsymbol{\sigma}} = \sum_{i=1}^{3} \frac{1}{2\breve{\mu}_i} \sigma_i \mathbf{N}_i \otimes \mathbf{N}_i - \frac{3}{\breve{\zeta}} p \mathbf{I} \tag{42}$$

and the associated *exact* and *symmetric* compliance tensor is

$$\mathbb{S} = \frac{d^2\check{\Psi}^c(\boldsymbol{\sigma})}{d\boldsymbol{\sigma}\otimes d\boldsymbol{\sigma}} = \sum_{i=1}^{3}\frac{1}{2\check{\mu}_i}\mathbb{N}_{iiii} + \sum_{i=1}^{3}\sum_{j\neq i}\frac{\frac{1}{2\check{\mu}_j}\sigma_j - \frac{1}{2\check{\mu}_i}\sigma_i}{\sigma_j-\sigma_i}\frac{1}{2}\left(\mathbb{N}_{ijij}+\mathbb{N}_{ijji}\right) - \frac{1}{\check{\zeta}}\mathbf{I}\otimes\mathbf{I} \tag{43}$$

2.6. Different generalizations of Hooke's law in principal directions

2.6.1. Uncoupled strain-driven bi-modulus formulation

The axial-to-axial components of Eq. (33) in principal directions and expressed in matrix notation read

$$[\mathbb{C}]_{\mathrm{N}} = \left[\mathbb{P}^d\right]\begin{bmatrix} 2\hat{\mu}_1 & 0 & 0\\ 0 & 2\hat{\mu}_2 & 0\\ 0 & 0 & 2\hat{\mu}_3\end{bmatrix}\left[\mathbb{P}^d\right] + \hat{K}\begin{bmatrix}1&1&1\\1&1&1\\1&1&1\end{bmatrix} \tag{44}$$

where

$$\left[\mathbb{P}^d\right] = \frac{1}{3}\begin{bmatrix}2&-1&-1\\-1&2&-1\\-1&-1&2\end{bmatrix} \tag{45}$$

or, in expanded form (where we define the mean, deformation-dependent shear moduli $3\hat{\mu}_m := \hat{\mu}_1+\hat{\mu}_2+\hat{\mu}_3$)

$$[\mathbb{C}]_{\mathrm{N}} = \frac{1}{3}\begin{bmatrix} 2\hat{\mu}_m+2\hat{\mu}_1 & -4\hat{\mu}_m+2\hat{\mu}_3 & -4\hat{\mu}_m+2\hat{\mu}_2\\ -4\hat{\mu}_m+2\hat{\mu}_3 & 2\hat{\mu}_m+2\hat{\mu}_2 & -4\hat{\mu}_m+2\hat{\mu}_1\\ -4\hat{\mu}_m+2\hat{\mu}_2 & -4\hat{\mu}_m+2\hat{\mu}_1 & 2\hat{\mu}_m+2\hat{\mu}_3\end{bmatrix} + \hat{K}\begin{bmatrix}1&1&1\\1&1&1\\1&1&1\end{bmatrix} \tag{46}$$

which, consistent with the hyperelasticity assumption, is symmetric by construction. Importantly, different specializations of this tensor are immediately obtained from its associated *strain* switches in Eqs. (12) and (13), i.e. respective signs of deviatoric principal strains and volumetric strain.

It can be readily shown that the inverse of the material stiffness matrix $[\mathbb{C}]_{\mathrm{N}}$ can also be

decomposed into deviatoric and volumetric parts, namely $[\mathbb{S}]_{\mathrm{N}} = [\mathbb{C}]_{\mathrm{N}}^{-1}$ reads

$$[\mathbb{S}]_{\mathrm{N}} = \left[\mathbb{P}^d\right] \begin{bmatrix} -\hat{s}_1 + 2\hat{s}_2 + 2\hat{s}_3 & 0 & 0 \\ 0 & 2\hat{s}_1 - \hat{s}_2 + 2\hat{s}_3 & 0 \\ 0 & 0 & 2\hat{s}_1 + 2\hat{s}_2 - \hat{s}_3 \end{bmatrix} \left[\mathbb{P}^d\right] + \frac{1}{9\hat{K}} \begin{bmatrix} 1 & 1 & 1 \\ 1 & 1 & 1 \\ 1 & 1 & 1 \end{bmatrix}$$

with the strain-based tension-compression compliances

$$\hat{s}_i = \frac{\hat{\mu}_i}{2\hat{\mu}_1\hat{\mu}_2 + 2\hat{\mu}_2\hat{\mu}_3 + 2\hat{\mu}_3\hat{\mu}_1} \ , \quad i = 1, 2, 3 \tag{47}$$

or, in expanded form

$$[\mathbb{S}]_{\mathrm{N}} = \begin{bmatrix} \hat{s}_2 + \hat{s}_3 & -\hat{s}_3 & -\hat{s}_2 \\ -\hat{s}_3 & \hat{s}_1 + \hat{s}_3 & -\hat{s}_1 \\ -\hat{s}_2 & -\hat{s}_1 & \hat{s}_1 + \hat{s}_2 \end{bmatrix} + \frac{1}{9\hat{K}} \begin{bmatrix} 1 & 1 & 1 \\ 1 & 1 & 1 \\ 1 & 1 & 1 \end{bmatrix} \tag{48}$$

By letting $[\varepsilon_1, \varepsilon_2, \varepsilon_3]^T = [\mathbb{S}]_{\mathrm{N}} [\sigma_1, \sigma_2, \sigma_3]^T$, we obtain the following generalized Hooke's law in principal directions for uncoupled strain-driven bi-modulus materials

$$\varepsilon_i = \left(\hat{s}_j + \hat{s}_k + \frac{1}{9\hat{K}}\right)\sigma_i - \left(\hat{s}_k - \frac{1}{9\hat{K}}\right)\sigma_j - \left(\hat{s}_j - \frac{1}{9\hat{K}}\right)\sigma_k \ , \quad i \neq j \neq k \neq i = 1, 2, 3 \tag{49}$$

2.6.2. Coupled strain-driven bi-modulus formulation

The axial-to-axial components of Eq. (37) in principal directions and expressed in matrix notation read

$$[\mathbb{C}]_{\mathrm{N}} = \begin{bmatrix} 2\bar{\mu}_1 + \bar{\lambda} & \bar{\lambda} & \bar{\lambda} \\ \bar{\lambda} & 2\bar{\mu}_2 + \bar{\lambda} & \bar{\lambda} \\ \bar{\lambda} & \bar{\lambda} & 2\bar{\mu}_3 + \bar{\lambda} \end{bmatrix} \tag{50}$$

Different specializations of this matrix are immediately obtained from its associated *strain* switches in Eqs. (15) and (16), i.e. respective signs of total principal strains and volumetric strain. The compliance matrix $[\mathbb{S}]_{\mathrm{N}} = [\mathbb{C}]_{\mathrm{N}}^{-1}$ reads (with $D = \frac{1}{2}\det[\mathbb{C}]_{\mathrm{N}} := 2\bar{\lambda}(\bar{\mu}_1\bar{\mu}_2 + \bar{\mu}_2\bar{\mu}_3 +$

$\bar{\mu}_3\bar{\mu}_1) + 4\bar{\mu}_1\bar{\mu}_2\bar{\mu}_3)$

$$[\mathbb{S}]_{\mathrm{N}} = \frac{1}{D}\begin{bmatrix} \bar{\lambda}(\bar{\mu}_2+\bar{\mu}_3)+2\bar{\mu}_2\bar{\mu}_3 & -\bar{\lambda}\bar{\mu}_3 & -\bar{\lambda}\bar{\mu}_2 \\ -\bar{\lambda}\bar{\mu}_3 & \bar{\lambda}(\bar{\mu}_1+\bar{\mu}_3)+2\bar{\mu}_1\bar{\mu}_3 & -\bar{\lambda}\bar{\mu}_1 \\ -\bar{\lambda}\bar{\mu}_2 & -\bar{\lambda}\bar{\mu}_1 & \bar{\lambda}(\bar{\mu}_1+\bar{\mu}_2)+2\bar{\mu}_1\bar{\mu}_2 \end{bmatrix} \tag{51}$$

which yields the following generalized Hooke's law in principal directions for coupled strain-driven bi-modulus materials

$$\varepsilon_i = \frac{\bar{\lambda}(\bar{\mu}_j+\bar{\mu}_k)+2\bar{\mu}_j\bar{\mu}_k}{D}\sigma_i - \frac{\bar{\lambda}\bar{\mu}_k}{D}\sigma_j - \frac{\bar{\lambda}\bar{\mu}_j}{D}\sigma_k \ , \quad i\neq j\neq k\neq i = 1,2,3 \tag{52}$$

2.6.3. Uncoupled stress-driven bi-modulus formulation

The axial-to-axial components of Eq. (40) in principal directions and expressed in matrix notation read

$$[\mathbb{S}]_{\mathrm{N}} = \left[\mathbb{P}^d\right]\begin{bmatrix} \frac{1}{2\tilde{\mu}_1} & 0 & 0 \\ 0 & \frac{1}{2\tilde{\mu}_2} & 0 \\ 0 & 0 & \frac{1}{2\tilde{\mu}_3} \end{bmatrix}\left[\mathbb{P}^d\right] + \frac{1}{9\tilde{K}}\begin{bmatrix} 1 & 1 & 1 \\ 1 & 1 & 1 \\ 1 & 1 & 1 \end{bmatrix} \tag{53}$$

or, in expanded form (where we define the mean, deformation-dependent shear moduli $3/(2\tilde{\mu}_m) := 1/(2\tilde{\mu}_1) + 1/(2\tilde{\mu}_2) + 1/(2\tilde{\mu}_3)$)

$$[\mathbb{S}]_{\mathrm{N}} = \frac{1}{3}\begin{bmatrix} \frac{1}{2\tilde{\mu}_m}+\frac{1}{2\tilde{\mu}_1} & -\frac{2}{2\tilde{\mu}_m}+\frac{1}{2\tilde{\mu}_3} & -\frac{2}{2\tilde{\mu}_m}+\frac{1}{2\tilde{\mu}_2} \\ -\frac{2}{2\tilde{\mu}_m}+\frac{1}{2\tilde{\mu}_3} & \frac{1}{2\tilde{\mu}_m}+\frac{1}{2\tilde{\mu}_2} & -\frac{2}{2\tilde{\mu}_m}+\frac{1}{2\tilde{\mu}_1} \\ -\frac{2}{2\tilde{\mu}_m}+\frac{1}{2\tilde{\mu}_2} & -\frac{2}{2\tilde{\mu}_m}+\frac{1}{2\tilde{\mu}_1} & \frac{1}{2\tilde{\mu}_m}+\frac{1}{2\tilde{\mu}_3} \end{bmatrix} + \frac{1}{9\tilde{K}}\begin{bmatrix} 1 & 1 & 1 \\ 1 & 1 & 1 \\ 1 & 1 & 1 \end{bmatrix} \tag{54}$$

Different specializations of this matrix are immediately obtained from its associated *stress* switches in Eqs. (25) and (26), i.e. respective signs of deviatoric principal stresses and volumetric stress. We obtain the following generalized Hooke's law in principal directions for uncoupled stress-driven bi-modulus materials

$$\varepsilon_i = \frac{1}{9}\left(\frac{3}{2\tilde{\mu}_m}+\frac{3}{2\tilde{\mu}_i}+\frac{1}{\tilde{K}}\right)\sigma_i - \frac{1}{9}\left(\frac{6}{2\tilde{\mu}_m}-\frac{3}{2\tilde{\mu}_k}-\frac{1}{\tilde{K}}\right)\sigma_j - \frac{1}{9}\left(\frac{6}{2\tilde{\mu}_m}-\frac{3}{2\tilde{\mu}_j}-\frac{1}{\tilde{K}}\right)\sigma_k \tag{55}$$

2.6.4. Coupled stress-driven bi-modulus formulation

The axial-to-axial components of Eq. (43) in principal directions and expressed in matrix notation read

$$[\mathbb{S}]_{\mathrm{N}} = \begin{bmatrix} \frac{1}{2\check{\mu}_1} - \frac{1}{\check{\zeta}} & -\frac{1}{\check{\zeta}} & -\frac{1}{\check{\zeta}} \\ -\frac{1}{\check{\zeta}} & \frac{1}{2\check{\mu}_2} - \frac{1}{\check{\zeta}} & -\frac{1}{\check{\zeta}} \\ -\frac{1}{\check{\zeta}} & -\frac{1}{\check{\zeta}} & \frac{1}{2\check{\mu}_3} - \frac{1}{\check{\zeta}} \end{bmatrix} \tag{56}$$

Different specializations of this matrix are immediately obtained from its associated *stress* switches in Eqs. (28) and (29), i.e. respective signs of total principal stresses and volumetric stress. We obtain the following generalized Hooke's law in principal directions for coupled stress-driven bi-modulus materials

$$\varepsilon_i = \left(\frac{1}{2\check{\mu}_i} - \frac{1}{\check{\zeta}}\right)\sigma_i - \frac{1}{\check{\zeta}}\left(\sigma_j + \sigma_k\right) \ , \quad i \neq j \neq k \neq i = 1,2,3 \tag{57}$$

Finally, it is straightforward to show that all four previous strain-stress relations, namely Eqs. (49), (52), (55), and (57), recover Hooke's law $\varepsilon_i = \frac{1}{E}\sigma_i - \frac{\nu}{E}(\sigma_j + \sigma_k)$ (depending on two constants) for linear isotropic materials.

Remark 1. *Equation (57) represents, importantly, a generalization of a widely used model for a* subset *of coupled stress-driven bi-modulus materials, namely Ambartsumyan's model [26] (cf. Ref. [31] and references therein)*

$$\varepsilon_i = \frac{1}{E^+}\sigma_i - C_0\left(\sigma_j + \sigma_k\right) \ , \quad \textit{if } \sigma_i > 0 \tag{58}$$

$$\varepsilon_i = \frac{1}{E^-}\sigma_i - C_0\left(\sigma_j + \sigma_k\right) \ , \quad \textit{if } \sigma_i \leq 0 \tag{59}$$

with $i \neq j \neq k \neq i = 1,2,3$. In this regard, note that Ambartsumyan's model, first, depends on three independent constants (E^+, E^-, C_0), rather than four ($\check{\mu}^+$, $\check{\mu}^-$, $\check{\zeta}^+$, $\check{\zeta}^-$), and, second, is based on a single type of switches (for total stresses σ_i), rather than two types of simultaneous switches (for total stresses σ_i and hydrostatic pressure p).

2.7. Determination of material parameters

We determine here all the previous models, depending on four material parameters each, from four experimental values, typically stress-strain or strain-strain slopes, obtained from a complete tension-compression uniaxial test.

2.7.1. Uncoupled strain-driven bi-modulus formulation

Consider a uniaxial tension test in direction 1, i.e. $\varepsilon_1 \equiv \varepsilon > 0$, for which we define the (apparent, external) tensile Young modulus E^+ and Poisson ratio ν^+ such that $\sigma_1 = E^+\varepsilon_1$ and $\varepsilon_2 = \varepsilon_3 = -\nu^+\varepsilon_1$. In this case

$$\varepsilon^v = \varepsilon_1 - 2\nu^+\varepsilon_1 = \left(1 - 2\nu^+\right)\varepsilon \tag{60}$$

$$\varepsilon_1^d = \varepsilon_1 - \frac{1}{3}\varepsilon^v = \frac{2}{3}\left(1 + \nu^+\right)\varepsilon \tag{61}$$

so both ε_1^d and ε_v are positive if $-1 < \nu^+ < 1/2$, as we consider next. Hence, $\hat{\mu}_1 = \hat{\mu}^+$ (because $\varepsilon_1^d > 0$) and $\hat{\mu}_2 = \hat{\mu}_3 = \hat{\mu}^-$ (because $\varepsilon_2^d = \varepsilon_3^d = -\varepsilon_1^d/2 < 0$), as well as $\hat{K} = \hat{K}^+$ (because $\varepsilon^v > 0$), so axial-to-axial components of the compliance tensor $\mathbb{S}$ in Eq. (48) reduce to

$$[\mathbb{S}]_{\mathrm{N}} = \frac{1}{2\hat{\mu}^-\left(2\hat{\mu}^+ + \hat{\mu}^-\right)}\begin{bmatrix} 2\hat{\mu}^- & -\hat{\mu}^- & -\hat{\mu}^- \\ -\hat{\mu}^- & \hat{\mu}^+ + \hat{\mu}^- & -\hat{\mu}^+ \\ -\hat{\mu}^- & -\hat{\mu}^+ & \hat{\mu}^+ + \hat{\mu}^- \end{bmatrix} + \frac{1}{9\hat{K}^+}\begin{bmatrix} 1 & 1 & 1 \\ 1 & 1 & 1 \\ 1 & 1 & 1 \end{bmatrix} \tag{62}$$

such that

$$\begin{bmatrix} \varepsilon_1 \\ \varepsilon_2 \\ \varepsilon_3 \end{bmatrix} = \frac{1}{E^+}\begin{bmatrix} 1 \\ -\nu^+ \\ -\nu^+ \end{bmatrix}\sigma_1 = [\mathbb{S}]\begin{bmatrix} \sigma_1 \\ 0 \\ 0 \end{bmatrix} \tag{63}$$

i.e.

$$\frac{1}{E^+}\begin{bmatrix} 1 \\ -\nu^+ \\ -\nu^+ \end{bmatrix} = \frac{1}{2\hat{\mu}^+ + \hat{\mu}^-}\begin{bmatrix} 1 \\ -1/2 \\ -1/2 \end{bmatrix} + \frac{1}{9\hat{K}^+}\begin{bmatrix} 1 \\ 1 \\ 1 \end{bmatrix} \tag{64}$$

which gives the following relations for uncoupled strain-driven bi-modulus materials

$$E^+ = \frac{\left(2\hat{\mu}^+ + \hat{\mu}^-\right)9\hat{K}^+}{2\hat{\mu}^+ + \hat{\mu}^- + 9\hat{K}^+} \tag{65}$$

and

$$\nu^+ = \frac{-4\hat{\mu}^+ - 2\hat{\mu}^- + 9\hat{K}^+}{4\hat{\mu}^+ + 2\hat{\mu}^- + 18\hat{K}^+} \tag{66}$$

It is straightforward to verify for a uniaxial compression test in direction 1 (i.e., $\varepsilon_1 < 0$), for which we define the compression Young modulus E^- and Poisson ratio ν^-, that the following relations are obtained

$$E^- = \frac{(2\hat{\mu}^- + \hat{\mu}^+)\, 9\hat{K}^-}{2\hat{\mu}^- + \hat{\mu}^+ + 9\hat{K}^-} \tag{67}$$

and

$$\nu^- = \frac{-4\hat{\mu}^- - 2\hat{\mu}^+ + 9\hat{K}^-}{4\hat{\mu}^- + 2\hat{\mu}^+ + 18\hat{K}^-} \tag{68}$$

Therefore, again, an alternative set of *four* generally independent material constants (E^+, E^-, ν^+, and ν^-) can be used to define a bi-linear elastic isotropic material.

Nevertheless, what one usually seeks to determine is the shear bi-modulus and bulk bi-modulus (i.e., the model parameters) from experimentally measured Young bi-modulus and Poisson bi-ratio. Equations (65)-(68) give such relations, namely

$$\hat{\mu}^+ = \frac{E^+}{1+\nu^+} - \frac{1}{2}\frac{E^-}{1+\nu^-} \tag{69}$$

$$\hat{\mu}^- = \frac{E^-}{1+\nu^-} - \frac{1}{2}\frac{E^+}{1+\nu^+} \tag{70}$$

and

$$\hat{K}^+ = \frac{1}{3}\frac{E^+}{1-2\nu^+} \tag{71}$$

$$\hat{K}^- = \frac{1}{3}\frac{E^-}{1-2\nu^-} \tag{72}$$

which specialize to $2\mu = E/(1+\nu)$ and $3K = E/(1-2\nu)$ for $E^+ = E^- \equiv E$ and $\nu^+ = \nu^- \equiv \nu$.

2.7.2. Coupled strain-driven bi-modulus formulation

Following similar steps as above, for both tension and compression uniaxial tests, the following relations for coupled strain-driven bi-modulus materials are obtained

$$E^+ = \frac{\bar{\lambda}^+ \left(2\bar{\mu}^+ + \bar{\mu}^-\right) + 2\bar{\mu}^+\bar{\mu}^-}{\bar{\lambda}^+ + \bar{\mu}^-} \quad \text{and} \quad E^- = \frac{\bar{\lambda}^- \left(2\bar{\mu}^- + \bar{\mu}^+\right) + 2\bar{\mu}^-\bar{\mu}^+}{\bar{\lambda}^- + \bar{\mu}^+} \tag{73}$$

as well as

$$\nu^+ = \frac{1}{2}\frac{\bar{\lambda}^+}{\bar{\lambda}^+ + \bar{\mu}^-} \quad \text{and} \quad \nu^- = \frac{1}{2}\frac{\bar{\lambda}^-}{\bar{\lambda}^- + \bar{\mu}^+} \tag{74}$$

which define the model parameters $\bar{\mu}^+$, $\bar{\mu}^-$, $\bar{\lambda}^+$, $\bar{\lambda}^-$ from the experimental values E^+, E^-, ν^+, ν^-

$$\bar{\mu}^+ = \frac{1}{2}\frac{E^+ - \nu^+ E^-}{1 - \nu^+\nu^-} \tag{75}$$

$$\bar{\mu}^- = \frac{1}{2}\frac{E^- - \nu^- E^+}{1 - \nu^+\nu^-} \tag{76}$$

and

$$\bar{\lambda}^+ = \frac{\left(E^- - \nu^- E^+\right)\nu^+}{\left(1 - \nu^+\nu^-\right)\left(1 - 2\nu^+\right)} \tag{77}$$

$$\bar{\lambda}^- = \frac{\left(E^+ - \nu^+ E^-\right)\nu^-}{\left(1 - \nu^+\nu^-\right)\left(1 - 2\nu^-\right)} \tag{78}$$

which specialize to $2\mu = E/(1+\nu)$ and $\lambda = E\nu/\left(\left(1+\nu\right)\left(1-2\nu\right)\right)$ for linear elasticity. As mentioned above, note that $\hat{\mu}^+ \neq \bar{\mu}^+$ or $\hat{\mu}^- \neq \bar{\mu}^-$ for given E^+, E^-, ν^+, ν^-, in general.

2.7.3. Uncoupled stress-driven bi-modulus formulation

Following similar steps, the following relations for uncoupled stress-driven bi-modulus materials are obtained

$$E^+ = \frac{9\tilde{K}^+\tilde{\mu}^+\tilde{\mu}^-}{\tilde{\mu}^+\tilde{\mu}^- + \tilde{K}^+\tilde{\mu}^+ + 2\tilde{K}^+\tilde{\mu}^-} \quad \text{and} \quad E^- = \frac{9\tilde{K}^-\tilde{\mu}^-\tilde{\mu}^+}{\tilde{\mu}^-\tilde{\mu}^+ + \tilde{K}^-\tilde{\mu}^- + 2\tilde{K}^-\tilde{\mu}^+} \tag{79}$$

as well as

$$\nu^+ = \frac{1}{2}\frac{\tilde{K}^+\left(\tilde{\mu}^+ + 2\tilde{\mu}^-\right) - 2\tilde{\mu}^+\tilde{\mu}^-}{\tilde{\mu}^+\tilde{\mu}^- + \tilde{K}^+\tilde{\mu}^+ + 2\tilde{K}^+\tilde{\mu}^-} \quad \text{and} \quad \nu^- = \frac{1}{2}\frac{\tilde{K}^-\left(\tilde{\mu}^- + 2\tilde{\mu}^+\right) - 2\tilde{\mu}^-\tilde{\mu}^+}{\tilde{\mu}^-\tilde{\mu}^+ + \tilde{K}^-\tilde{\mu}^- + 2\tilde{K}^-\tilde{\mu}^+} \tag{80}$$

which define the model parameters $\tilde{\mu}^+$, $\tilde{\mu}^-$, $\tilde{\lambda}^+$, $\tilde{\lambda}^-$ from the experimental values E^+, E^-, ν^+, ν^-

$$\tilde{\mu}^+ = \frac{E^+E^-}{-2E^+ + 4E^- - 2\nu^-E^+ + 4\nu^+E^-} \tag{81}$$

$$\tilde{\mu}^- = \frac{E^+E^-}{-2E^- + 4E^+ - 2\nu^+E^- + 4\nu^-E^+} \tag{82}$$

and

$$\tilde{K}^+ = \frac{1}{3}\frac{E^+}{1-2\nu^+} \tag{83}$$

$$\tilde{K}^- = \frac{1}{3}\frac{E^-}{1-2\nu^-} \tag{84}$$

which specialize to $2\mu = E/(1+\nu)$ and $3K = E/(1-2\nu)$ for $E^+ = E^- \equiv E$ and $\nu^+ = \nu^- \equiv \nu$. Note that both, strain- and stress-based, uncoupled formulations have the same bulk bi-modulus values $\tilde{K}^+ = \hat{K}^+$ and $\tilde{K}^- = \hat{K}^-$ but, in general, different shear bi-modulus $\tilde{\mu}^+ \neq \hat{\mu}^+$ and $\tilde{\mu}^- \neq \hat{\mu}^-$, compare Eqs. (69)-(72) to (81)-(84).

2.7.4. Coupled stress-driven bi-modulus formulation

Following similar steps, the following relations for coupled stress-driven bi-modulus materials are obtained

$$E^+ = \frac{2\breve{\mu}^+\breve{\zeta}^+}{\breve{\zeta}^+ - 2\breve{\mu}^+} \quad \text{and} \quad E^- = \frac{2\breve{\mu}^-\breve{\zeta}^-}{\breve{\zeta}^- - 2\breve{\mu}^-} \tag{85}$$

as well as

$$\nu^+ = \frac{2\breve{\mu}^+}{\breve{\zeta}^+ - 2\breve{\mu}^+} \quad \text{and} \quad \nu^- = \frac{2\breve{\mu}^-}{\breve{\zeta}^- - 2\breve{\mu}^-} \tag{86}$$

which define the model parameters $\breve{\mu}^+$, $\breve{\mu}^-$, $\breve{\lambda}^+$, $\breve{\lambda}^-$ from the experimental values E^+, E^-, ν^+, ν^-

$$\breve{\mu}^+ = \frac{E^+}{2\,(1+\nu^+)} \tag{87}$$

$$\breve{\mu}^- = \frac{E^-}{2\,(1+\nu^-)} \tag{88}$$

and

$$\breve{\zeta}^+ = \frac{E^+}{\nu^+} \tag{89}$$

$$\breve{\zeta}^- = \frac{E^-}{\nu^-} \tag{90}$$

which specialize to $2\mu = E/(1+\nu)$ and $\zeta = E/\nu$ for linear elasticity.

Remark 2. *For the particular case of coupled stress-driven bi-modulus materials, note that, in general*

$$\frac{E^+}{\nu^+} = \breve{\zeta}^+ \neq \breve{\zeta}^- = \frac{E^-}{\nu^-} \tag{91}$$

Hence, Ambartsumyan's model [26], for which

$$\frac{E^+}{\nu^+} = \frac{1}{C_0} = \frac{E^-}{\nu^-} \tag{92}$$

in Eqs. (58) and (59), represents a particular case of the coupled stress-driven formulation for which the volumetric stress switch in Eq. (29) is not required because both Lamé compliance moduli ($\breve{\zeta}^+$ and $\breve{\zeta}^-$) are implicitly assumed *to collapse to a single one ($1/C_0$). Furthermore, E^+ (if $\sigma_i > 0$) and E^- (if $\sigma_i < 0$) in Eqs. (58) and (59) consistently relate to $\breve{\mu}^+$ (if $\sigma_i > 0$) and $\breve{\mu}^-$ (if $\sigma_i < 0$) through Eq. (85) with $\breve{\zeta} \equiv \breve{\zeta}^+ = \breve{\zeta}^-$, see also Eq. (57). We remark, however, that this simplifying assumption is not necessarily satisfied by actual bi-modulus materials, for which two independent switches are* simultaneously *needed to determine the two independent moduli that are* simultaneously *active at a given stress-strain state. In this respect, we note that the symmetrizing assumption $\nu^+/E^+ = \nu^-/E^-$ is not generally satisfied by any of the uncoupled or coupled, strain- or stress-driven bi-modulus hyperelastic*

formulations presented in this work.

2.8. Extension to finite strains

The previous formulations may be extended to the finite strain framework in a quite straightforward manner by using logarithmic strains $\mathbf{E}$ and the work-conjugate [45] generalized Kirchhoff stresses $\mathbf{T}$, which are equal to the rotated Kirchhoff stresses in the case of isotropy [46]. Material logarithmic strains are defined as the logarithm of the right stretch tensor $\mathbf{U}$, i.e. $\mathbf{E} = \ln \mathbf{U}$, so the principal logarithmic strains are the logarithm of the corresponding stretches, $\ln(\lambda_i)$. It has been shown that in a general case, they can be interpreted as the integral of differential infinitesimal strains along specific paths [47]. Then, it is immediate to verify that most operators are the same for infinitesimal and logarithmic strains; e.g. volumetric and deviatoric logarithmic strains are, respectively

$$E^v = \mathbf{E} : \mathbf{I} = \ln \lambda_1 + \ln \lambda_2 + \ln \lambda_3 = \ln J \tag{93}$$

$$\mathbf{E}^d = \mathbf{E} - \tfrac{1}{3} E^v \mathbf{I} = diag \left[\ln(J^{-\frac{1}{3}} \lambda_1), \ln(J^{-\frac{1}{3}} \lambda_2), \ln(J^{-\frac{1}{3}} \lambda_3) \right] \tag{94}$$

where $\mathbf{E}^d$ has the diagonal matrix representation in principal directions, with principal values $E_i^d := \ln(\lambda_i^d) = \ln(J^{-\frac{1}{3}} \lambda_i)$, where λ_i^d are the isochoric stretches; i.e. $\lambda_1^d \lambda_2^d \lambda_3^d = 1$, and J is the Jacobian of the finite deformation. Similar parallelism can be found between $\boldsymbol{\sigma}$ and $\mathbf{T}$. Then, the previous formulations may be extended to finite strains replacing $\boldsymbol{\varepsilon}$ by $\mathbf{E}$ and $\boldsymbol{\sigma}$ by $\mathbf{T}$. This approach is common in finite strain multiplicative elasto-plasticity to preserve the simple structure of infinitesimal strain algorithms at large strains; see e.g. [48–51], and [52] for visco-hyperelasticity, among others. The extension to anisotropic cases is slightly more elaborate because material invariants must be used (for example in symmetry planes [53, 54]) instead of principal strains, and material-symmetries congruency should be taken into account [55].

However, we note that logarithmic strains are nonlinear functions of the displacements, so a fully nonlinear model is obtained. In this case, little advantage is obtained respect a classical hyperelastic model: note that spline-based hyperelasticity allows for abrupt changes in material moduli [44].

3. Predictions for additional tests: Determining the model to use

We show here that once the four material parameters for each model have been determined from four known experimental values (i.e., from two bi-linear experimental responses), predicted responses for additional tests given by different tension-compression models may result different. The predictive capability of each model for additional tests may serve then to identify which model, from the four addressed above, is better suited for the specific material under study.

3.1. Uncoupled strain-driven bi-modulus formulation

Consider, as an illustrative shear example, a (simple) shear test performed in a plane xy of a Cartesian reference frame $X_{xyz} = \{x, y, z\}$, for which $\varepsilon_{xy} = \varepsilon_{yx} = \gamma/2$, with γ the so-called angular distortion or engineering (orthogonal) shear strain, and all other components of $\boldsymbol{\varepsilon}$ being zero. Principal strain components, e.g. 1 and 2, in the plane xy are

$$\varepsilon_1 = -\varepsilon_2 = \gamma/2 > 0 \tag{95}$$

along with $\varepsilon_3 = 0$. Then, of course, $\varepsilon^v = \mathrm{tr}\,\boldsymbol{\varepsilon} = 0$, so $\boldsymbol{\varepsilon} \equiv \boldsymbol{\varepsilon}^d$, i.e. $\varepsilon_1^d = -\varepsilon_2^d = \gamma/2$ with respective moduli $\hat{\mu}_1 = \hat{\mu}^+$ and $\hat{\mu}_2 = \hat{\mu}^-$. The associated shear modulus $\hat{G}_{12}$ in the plane defined by $i = 1$ and $j = 2$ in Eq. (34) is, for uncoupled strain-driven bi-modulus materials

$$\hat{G}_{12} = \frac{\hat{\mu}_2\varepsilon_2^d - \hat{\mu}_1\varepsilon_1^d}{\varepsilon_2^d - \varepsilon_1^d} = \frac{\hat{\mu}^-\varepsilon_2^d + \hat{\mu}^+\varepsilon_2^d}{\varepsilon_2^d + \varepsilon_2^d} = \frac{\hat{\mu}^- + \hat{\mu}^+}{2} = \frac{1}{4}\left(\frac{E^+}{1+\nu^+} + \frac{E^-}{1+\nu^-}\right) \tag{96}$$

where we used Eqs. (69) and (70).

3.2. Coupled strain-driven bi-modulus formulation

Following similar steps as for the uncoupled strain-driven formulation, for a shear test, the following shear modulus $\bar{G}_{12}$ in Eq. (37) is obtained for coupled strain-driven bi-modulus materials

$$\bar{G}_{12} = \frac{\bar{\mu}_2\varepsilon_2 - \bar{\mu}_1\varepsilon_1}{\varepsilon_2 - \varepsilon_1} = \frac{\bar{\mu}^-\varepsilon_2^d + \bar{\mu}^+\varepsilon_2^d}{\varepsilon_2^d + \varepsilon_2^d} = \frac{\bar{\mu}^- + \bar{\mu}^+}{2} = \frac{1}{4}\frac{E^+\left(1-\nu^-\right) + E^-\left(1-\nu^+\right)}{1-\nu^+\nu^-} \tag{97}$$

where we used Eqs. (75) and (76).

3.3. Uncoupled stress-driven bi-modulus formulation

For a shear test as the one considered above, Eq. (38), with $[\boldsymbol{\varepsilon}]_{\rm N}^T = [\varepsilon_1, \varepsilon_2, 0]^T$ and $\varepsilon_1 = -\varepsilon_2 = \varepsilon_{xy} > 0$, yields in principal directions

$$[\boldsymbol{\varepsilon}]_{\rm N}^T = \begin{bmatrix} \varepsilon_{xy} \\ -\varepsilon_{xy} \\ 0 \end{bmatrix}^T = \frac{1}{3} \begin{bmatrix} \dfrac{\sigma_1^d}{2\tilde{\mu}^+} \\ \dfrac{\sigma_2^d}{2\tilde{\mu}^-} \\ \dfrac{\sigma_3^d}{2\tilde{\mu}_3} \end{bmatrix}^T \begin{bmatrix} 2 & -1 & -1 \\ -1 & 2 & -1 \\ -1 & -1 & 2 \end{bmatrix} = \frac{1}{6} \begin{bmatrix} \dfrac{2\sigma_1^d}{\tilde{\mu}^+} - \dfrac{\sigma_2^d}{\tilde{\mu}^-} - \dfrac{\sigma_3^d}{\tilde{\mu}_3} \\ \dfrac{2\sigma_2^d}{\tilde{\mu}^-} - \dfrac{\sigma_3^d}{\tilde{\mu}_3} - \dfrac{\sigma_1^d}{\tilde{\mu}^+} \\ \dfrac{2\sigma_3^d}{\tilde{\mu}_3} - \dfrac{\sigma_1^d}{\tilde{\mu}^+} - \dfrac{\sigma_2^d}{\tilde{\mu}^-} \end{bmatrix}^T \tag{98}$$

which, with $\sigma_1^d + \sigma_2^d + \sigma_3^d = 0$, yields

$$\frac{\sigma_1^d}{\varepsilon_{xy}} = \frac{6\tilde{\mu}^+\tilde{\mu}^-}{2\tilde{\mu}^- + \tilde{\mu}^+}\,, \quad \frac{\sigma_2^d}{\varepsilon_{xy}} = -\frac{(2\tilde{\mu}^+ + \tilde{\mu}^-)\,2\tilde{\mu}^-}{2\tilde{\mu}^- + \tilde{\mu}^+} \quad \text{and} \quad \frac{\sigma_3^d}{\varepsilon_{xy}} = -2\tilde{\mu}_3 \frac{\tilde{\mu}^+ - \tilde{\mu}^-}{\tilde{\mu}^+ + \tilde{\mu}^- + \tilde{\mu}_3} \tag{99}$$

so, if, for example, $\tilde{\mu}^+ > \tilde{\mu}^- > 0$

$$\sigma_3^d < 0 \implies \tilde{\mu}_3 = \tilde{\mu}^- \tag{100}$$

Note also that $\tilde{\mu}_1 = \tilde{\mu}^+$ (because $\sigma_1^d > 0$) and $\tilde{\mu}_2 = \tilde{\mu}^-$ (because $\sigma_2^d < 0$), as assumed initially. The following shear modulus $\tilde{G}_{12}$ in Eq. (41) is obtained for uncoupled stress-driven bi-modulus materials (with $\tilde{\mu}^+ > \tilde{\mu}^-$)

$$\tilde{G}_{12} = \frac{\sigma_1^d - \sigma_2^d}{\sigma_1^d/\tilde{\mu}^+ - \sigma_2^d/\tilde{\mu}^-} = \frac{\tilde{\mu}^-\,(5\tilde{\mu}^+ + \tilde{\mu}^-)}{4\tilde{\mu}^- + 2\tilde{\mu}^+} = \tilde{G}_{12}(E^+, E^-, \nu^+, \nu^-) \tag{101}$$

where the relation $\tilde{G}_{12}(E^+, E^-, \nu^+, \nu^-)$ is obtained from Eqs. (81) and (82).

3.4. Coupled stress-driven bi-modulus formulation

For a shear test as the one considered above, Eq. (42) yields in principal directions

$$[\boldsymbol{\varepsilon}]_{\rm N} = \begin{bmatrix} \varepsilon_1 \\ \varepsilon_2 \\ \varepsilon_3 \end{bmatrix} = \begin{bmatrix} \varepsilon_{xy} \\ -\varepsilon_{xy} \\ 0 \end{bmatrix} = \begin{bmatrix} \dfrac{\sigma_1}{2\breve{\mu}^+} - \dfrac{\sigma_1 + \sigma_2 + \sigma_3}{\breve{\zeta}} \\ \dfrac{\sigma_2}{2\breve{\mu}^-} - \dfrac{\sigma_1 + \sigma_2 + \sigma_3}{\breve{\zeta}} \\ \dfrac{\sigma_3}{2\breve{\mu}_3} - \dfrac{\sigma_1 + \sigma_2 + \sigma_3}{\breve{\zeta}} \end{bmatrix} \tag{102}$$

which yields

$$\frac{\sigma_1}{\varepsilon_{xy}} = 2\check{\mu}^+ \frac{\check{\zeta} - 4\check{\mu}^- - 2\check{\mu}_3}{\check{\zeta} - 2\check{\mu}^+ - 2\check{\mu}^- - 2\check{\mu}_3} \ , \quad \frac{\sigma_2}{\varepsilon_{xy}} = -2\check{\mu}^- \frac{\check{\zeta} - 4\check{\mu}^+ - 2\check{\mu}_3}{\check{\zeta} - 2\check{\mu}^+ - 2\check{\mu}^- - 2\check{\mu}_3} \tag{103}$$

and

$$\frac{\sigma_3}{\varepsilon_{xy}} = 4\check{\mu}_3 \frac{\check{\mu}^+ - \check{\mu}^-}{\check{\zeta} - 2\check{\mu}^+ - 2\check{\mu}^- - 2\check{\mu}_3} \tag{104}$$

so, if, for example, $\check{\mu}^+ > \check{\mu}^- > 0$ and $\check{\zeta}^+ > 6\check{\mu}^+$

$$\sigma_3 > 0 \implies \check{\mu}_3 = \check{\mu}^+ \tag{105}$$

and

$$p \propto (\check{\mu}^+ - \check{\mu}^-) > 0 \implies \check{\zeta} = \check{\zeta}^+ \tag{106}$$

which is also consistent with $\check{\mu}_1 = \check{\mu}^+$ (i.e., $\sigma_1 > 0$) and $\check{\mu}_2 = \check{\mu}^-$ (i.e., $\sigma_2 < 0$), as assumed initially. The following shear modulus $\check{G}_{12}$ in Eq. (43) is obtained for coupled stress-driven bi-modulus materials (with $\check{\mu}^+ > \check{\mu}^-$ and $\check{\zeta}^+ > 6\check{\mu}^+$)

$$\check{G}_{12} = \frac{\sigma_1 - \sigma_2}{\sigma_1/\check{\mu}^+ - \sigma_2/\check{\mu}^-} = \frac{\check{\zeta}^+ (\check{\mu}^+ + \check{\mu}^-) - 2\check{\mu}^+ (\check{\mu}^+ + 5\check{\mu}^-)}{2\check{\zeta}^+ - 8\check{\mu}^+ - 4\check{\mu}^-} = \check{G}_{12}(E^+, E^-, \nu^+, \nu^-) \tag{107}$$

where the relation $\check{G}_{12}(E^+, E^-, \nu^+, \nu^-)$ is obtained from Eqs. (87)-(90).

4. Stress-driven vs. strain-driven procedures

It has been recently submitted that a stress-driven, rather than strain-driven, formulation should be used when dealing with bi-modulus materials, with a heuristic proof given in Remark 1 in Ref. [40], based on the example in Fig. 5 therein. We show next that, for example, an uncoupled strain-driven approach based on deviatoric and volumetric strain components and respective shear and bulk bi-moduli, constitutes an alternative systematic procedure to determine the *three-dimensional* tension-compression state of the material along principal directions. Albeit not addressed in detail, a similar reasoning follows for the coupled strain-driven approach.

Considering the laterally constrained uniaxial test in Fig. 5 in Ref. [40], which we

assume is performed along principal direction 1 (with $\varepsilon_1 \equiv \varepsilon_u > 0$) and constrained on both lateral directions 2 and 3, one obtains that the transverse strains $\varepsilon_2 = \varepsilon_3 \equiv \varepsilon_t$ are such that $-\nu^+ \leq \varepsilon_t/\varepsilon_u \leq 0$, where the lower limit $-\nu^+$ describes a laterally unconstrained uniaxial test (see Eq. (63)) and the higher limit 0 describes a test under total lateral restriction. Then, since ε_t are, in general, negative, but the lateral tensile force exerted over the body is, in general, positive, the authors in Ref. [40] conclude that "principle stresses rather than principle strains should be employed to determine the tensile or compressive status of a material point along a specific principal direction". The authors apparently refer to total strains. However, we show next that deviatoric and volumetric components of strain, either positive or negative, can be systematically employed for such a task.

For simplicity, consider the case completely constrained laterally. Then, $\varepsilon_u > 0$ and $\varepsilon_t = 0$, so $e = \varepsilon_u > 0$, $\varepsilon_u^d = \frac{2}{3}\varepsilon_u > 0$ and $\varepsilon_t^d = -\frac{1}{3}\varepsilon_u < 0$, whereupon $\hat{K} = \hat{K}^+$, $\hat{\mu}_u = \hat{\mu}^+$ and $\hat{\mu}_t = \hat{\mu}^-$. Hence, in contrast to the observation in Remark 1 in Ref. [40], note that one can indeed consider a compression constant in transverse directions (i.e., $\hat{\mu}_t = \hat{\mu}^-$) even if $\sigma_t > 0$. Axial and transverse equations, obtained from Eq. (31) for example, reduce to

$$\sigma_u = \left(\hat{K}^+ + \frac{8\hat{\mu}^+ + 4\hat{\mu}^-}{9}\right)\varepsilon_u \tag{108}$$

$$\sigma_t = \left(\hat{K}^+ - \frac{4\hat{\mu}^+ + 2\hat{\mu}^-}{9}\right)\varepsilon_u \tag{109}$$

or, using relations in Eqs. (69)-(71)

$$\sigma_u = \frac{E^+\left(1-\nu^+\right)}{\left(1+\nu^+\right)\left(1-2\nu^+\right)}\varepsilon_u \tag{110}$$

$$\sigma_t = \frac{E^+\nu^+}{\left(1+\nu^+\right)\left(1-2\nu^+\right)}\varepsilon_u \tag{111}$$

which, note, ultimately depend on the tensile Young modulus E^+ and tensile Poisson ratio ν^+.

Finally, regarding general computational procedures associated with stress- or strain-driven approaches, note that a phenomenological generalization of the stress-driven framework in Ref. [40] does not seem optimal for (displacement-based) finite element implementations, leading to the iterative algorithm and elaborate tangents in Ref. [31] (see Fig. 2

and Appendix B therein, respectively); below we further address this issue. In contrast, both coupled and uncoupled strain-driven approaches are optimal for (displacement-based) finite element implementations, with stresses and exact material tangent moduli determined immediately once the strain-driven switches are evaluated. Indeed, bi-linear materials as the ones addressed in this work are just a special case of materially non-linear (elastic) materials [46]. Furthermore, the present uncoupled strain-driven framework is a special case of fully nonlinear (uncoupled) hyperelastic materials [43] and can be easily extended to anisotropic materials [53, 54]. Hence, asymptotic quadratic rates of convergence within Newton-Raphson iterative procedures at the quadrature points are guaranteed by construction of the bi-modulus constitutive theory developed herein without any further modification (cf. Ref. [31]), as we show in Section 6.

As mentioned, stress-driven approaches are not as well suited for finite element codes, since they require an additional local iterative loop to fulfill the compatibility equation. For instance, the strain $\boldsymbol{\varepsilon}(\boldsymbol{\sigma}) = d\Psi^c(\boldsymbol{\sigma})/d\boldsymbol{\sigma}$ cannot be computed directly because at the material routine level, the final stresses are unknown until global equilibrium is established in the structure. Indeed, element subroutines facilitate to the material subroutines the strains (obtained from the iterative displacements) and expect to receive the corresponding stresses and tangent moduli. Thus the following compatibility equation must be enforced between the (global) element-level strains $\boldsymbol{\varepsilon}^{\square}$ and the (local) iterative material-level strains $\boldsymbol{\varepsilon}^{[j]}(\boldsymbol{\sigma}^{[j]}) = d\Psi^c/d\boldsymbol{\sigma}^{[j]}$

$$\boldsymbol{\rho}^{[j]}(\boldsymbol{\sigma}^{[j]}) := \boldsymbol{\varepsilon}^{[j]}(\boldsymbol{\sigma}^{[j]}) - \boldsymbol{\varepsilon}^{\square} \rightarrow \mathbf{0} \tag{112}$$

Obviously this equation may be solved as usual through a Newton-Raphson scheme or similar scheme until convergence is attained locally, e.g.

$$\boldsymbol{\sigma}^{[j+1]} = \boldsymbol{\sigma}^{[j]} - \left[\frac{d\boldsymbol{\rho}^{[j]}(\boldsymbol{\sigma}^{[j]})}{d\boldsymbol{\sigma}^{[j]}}\right]^{-1} : (\boldsymbol{\varepsilon}^{[j]} - \boldsymbol{\varepsilon}^{\square}) = \boldsymbol{\sigma}^{[j]} - \mathbb{S}^{[j]-1} : (\boldsymbol{\varepsilon}^{[j]} - \boldsymbol{\varepsilon}^{\square}) \tag{113}$$

A similar iterative approach was needed to plot Figs. 5 and 6, where strains were prescribed, but no iterations were needed for Figs. 1 to 4. After the computation of the compatible stresses, the stresses and tangent $\mathbb{C}^{[j]} = \mathbb{S}^{[j]-1}$ fulfilling both the constitutive and compatibility relations are returned, the latter for the global (equilibrium) iterations. Therefore, this

scheme introduces a new local loop, not present even in nonlinear large-strain hyperelasticity, which may be avoided using strain-driven formulations, unless strictly needed for an accurate material behavior description. In finite element simulations performed below, including both homogeneous and non-homogeneous deformation states, the initial guess ($j = 0$) to start the iterative procedure in Eq. (113) also proved relevant, especially for relatively high differences between tension and compression moduli. In this respect, stresses computed using either uncoupled or coupled strain-driven formulations proved useful to initialize Eq. (112) for either uncoupled or coupled stress-driven formulations, respectively.

5. Uncoupled vs. coupled formulations

To understand the implications of employing coupled switches, consider a deformation case with a volumetric strain 3ϵ and a superposed pure shear strain γ. Note that this is a quite general deformation state in the sense that the two types of deformation modes (dilatational and distortional) are superimposed in terms of their own variables. Then $\varepsilon_1 = \gamma/2 + \epsilon$, $\varepsilon_2 = -\gamma/2 + \epsilon$ and $\varepsilon_3 = \epsilon$. Consider for now $\gamma/2 + \epsilon > 0$ and $-\gamma/2 + \epsilon < 0$. Then, the stresses are

$$\sigma_1 = 3\bar{\lambda}\epsilon + \mu^+(\gamma + 2\epsilon) \tag{114}$$

$$\sigma_2 = 3\bar{\lambda}\epsilon + \mu^-(-\gamma + 2\epsilon) \tag{115}$$

$$\sigma_3 = 3\bar{\lambda}\epsilon + 2\bar{\mu}_3\epsilon \tag{116}$$

The in-plane maximum shear stress is

$$\tau = \frac{\sigma_1 - \sigma_2}{2} = \frac{\mu^+ + \mu^-}{2}\gamma + (\mu^+ - \mu^-)\epsilon \tag{117}$$

In Figure 1 we plot these equations for a given range of values for γ and ϵ. For the case of the shear stresses, in Figure 2 we plot the shear stress surface. It is seen that there is not only a single change of slope in each curve, but several of them and with changing sign. Furthermore, those changes are at different combinations of γ and ε. Note that we only considered distortion in one plane, so the picture becomes more complicated under combined

distortions. Hence, convergence difficulties can be expected, or at least a lag in convergence speed. Furthermore, the material can only be considered a "bi-modulus" material because it is defined by two constants for two independent material parameters, but not because it shows two slopes during a (combined) test.

Noteworthy, if the same exercise is performed for the associated (strain-based) uncoupled model, we obtain the plots shown in Figures 3 and 4. It is clearly seen that the curves have only two slopes in all cases, and the switches and shear stresses are independent of the dilatation.

Employing uncoupled switches for stresses in the associated complementary energy, one obtains bi-linear schemes similar to those shown in Figs. 3 and 4.

We can compare the previous approaches also with Ambartsumyan's model results for the same analysis, which are shown in Figures 5 and 6. It is seen than in this case, not only the elastic constants are reduced by one, but the curves are not bi-linear, having several changes of slope, also present at different combinations of ϵ and γ. As before, cases with combined distortions in other planes, introduce even more changes of slopes. This may explain some of the difficulties continuously reported in all works using Ambartsumyan's approach and their variants.

6. Illustrative examples

We perform in this Section finite element simulations with the general-purpose finite element analysis software ADINA [56], where the different models have been programmed through a user-defined material subroutine based on a materially-nonlinear-only formulation under small displacements and strains [46].

6.1. Tension-compression uniaxial tests: verification of material models

Assume that we have measured both tensile and compression Young moduli and Poisson ratios from respective uniaxial tests performed in tension (from which we obtain $E^+ = \sigma_u^+/\varepsilon_u^+$ and $\nu^+ = -\varepsilon_t^+/\varepsilon_u^+$) and compression (from which we obtain $E^- = \sigma_u^-/\varepsilon_u^-$ and $\nu^- = -\varepsilon_t^-/\varepsilon_u^-$). In particular, consider "experimental" slopes

$$E^+ = 105\,\mathrm{MPa}\,,\ \nu^+ = 0.4,\ E^- = 48\,\mathrm{MPa}\,,\ \nu^- = 0.2 \tag{118}$$

We can subsequently determine the model parameters for the different formulations presented above, which are the only material parameters for our ADINA user-defined subroutine. We obtain from Eqs. (69)-(72)

$$\hat{\mu}^+ = 55\,\text{MPa}\,,\ \hat{\mu}^- = 2.5\,\text{MPa}\,,\ \hat{K}^+ = 175\,\text{MPa}\,,\ \hat{K}^- = 26.67\,\text{MPa} \tag{119}$$

or from Eqs. (75)-(78)

$$\bar{\mu}^+ = 46.63\,\text{MPa}\,,\ \bar{\mu}^- = 14.67\,\text{MPa}\,,\ \bar{\lambda}^+ = 58.70\,\text{MPa}\,,\ \bar{\lambda}^- = 31.09\,\text{MPa} \tag{120}$$

or from Eqs. (81)-(84)

$$\tilde{\mu}^+ = 300\,\text{MPa}\,,\ \tilde{\mu}^- = 13.64\,\text{MPa}\,,\ \tilde{K}^+ = 175\,\text{MPa}\,,\ \tilde{K}^- = 26.67\,\text{MPa} \tag{121}$$

or from Eqs. (87)-(90)

$$\check{\mu}^+ = 37.5\,\text{MPa}\,,\ \check{\mu}^- = 20\,\text{MPa}\,,\ \check{\zeta}^+ = 262.5\,\text{MPa}\,,\ \check{\zeta}^- = 240\,\text{MPa} \tag{122}$$

We have simulated four tension-compression uniaxial tests in ADINA using respective material constants in Eqs. (119)-(122). The finite element model consists of a single brick 8-node element, with displacement-driven faces (both extension and compression) along axis x, and displacement-free lateral faces (axes y and z). We show in Fig. 7 results for uniaxial stress $\sigma_u \equiv \sigma_{xx}$ and transverse strain $\varepsilon_t \equiv \varepsilon_{yy} = \varepsilon_{zz}$, respectively, as a function of the uniaxial strain $\varepsilon_u \equiv \varepsilon_{xx}$, all of them being principal components. One can easily observe in these figures that, effectively, $E^+ = \sigma_u^+/\varepsilon_u^+ = 105\,\text{MPa}$, $E^- = \sigma_u^-/\varepsilon_u^- = 48\,\text{MPa}$, $\nu^+ = -\varepsilon_t^+/\varepsilon_u^+ = 0.4$, and $\nu^- = -\varepsilon_t^-/\varepsilon_u^- = 0.2$ for all four material models, with all four response curves overlapping. The fact that the response curves obtained from the numerically simulated tension-compression uniaxial tests reproduce the initially assumed "experimental" responses serves as numerical verification of the consistency of the models in principal directions, specifically, between respective internal model parameters in Eqs. (119)-(122) and external material constants in Eq. (118).

Finally, different situations were encountered when analyzing the numerical convergence of the simulations. When no local change of constitutive behavior took place (i.e., for incremental steps within either the tension branch, preserving $\varepsilon_u > 0$, or the compression branch, preserving $\varepsilon_u < 0$), exact numerical solutions (up to machine precision) were obtained in a single Newton-Raphson global iteration for all four models, consistent with a linear finite element computation. On other hand, when a local change in constitutive behavior took place (i.e., for incremental steps from the tension to the compression branch, or vice versa), two initial iterations were required to re-adjust tangents, with the corresponding exact numerical solution obtained at the final Newton-Raphson global iteration (now within the corresponding branch) for all formulations.

6.2. Shear test

In this example, we simulate four (simple) shear tests in ADINA in a plane $x - y$, with y the glide plane and x the shearing direction, using respective material constants in Eqs. (119)-(122). The finite element model consists of a single brick 8-node element, with displacements of the four nodes on face with normal y being prescribed along direction x and all other degrees of freedom fixed. This discretization ensures uniform fields of strain and stress within the element, which enables a comparison between numerical outcomes and analytical calculations. In particular, Eqs. (96), (97), (101) and (107) yield respective shear modulus

$$\hat{G}_{xy} = \frac{\hat{\mu}^- + \hat{\mu}^+}{2} = 28.75\,\text{MPa} \ , \tag{123}$$

$$\bar{G}_{xy} = \frac{\bar{\mu}^- + \bar{\mu}^+}{2} = 30.65\,\text{MPa} \ , \tag{124}$$

$$\tilde{G}_{xy} = \frac{\tilde{\mu}^- \left(5\tilde{\mu}^+ + \tilde{\mu}^-\right)}{4\tilde{\mu}^- + 2\tilde{\mu}^+} = 31.54\,\text{MPa} \ , \tag{125}$$

and

$$\check{G}_{xy} = \frac{\check{\zeta}^+ \left(\check{\mu}^+ + \check{\mu}^-\right) - 2\check{\mu}^+ \left(\check{\mu}^+ + 5\check{\mu}^-\right)}{2\check{\zeta}^+ - 8\check{\mu}^+ - 4\check{\mu}^-} = 32.97\,\text{MPa} \tag{126}$$

We show in Fig. 8 results for shear stresses σ_{xy} as a function of the shear strain $-10^{-3} \leq \gamma_{xy} \leq 10^{-3}$. One can observe that, effectively, different numerical predictions for σ_{xy} at $\gamma_{xy} = 10^{-3}$ are consistent with respective analytical results given by $\sigma_{xy} = G_{xy}\gamma_{xy}$. In

addition, we show numerical predictions for axial stresses σ_{xx}, σ_{yy}, and σ_{zz}, which were also verified analytically. Note the different axial stress components that different models require for this (totally) imposed shear strain state, especially the out-of-plane stress σ_{zz}, which is negative for both uncoupled formulations (cf., e.g., Eq. (100), valid for $\tilde{\mu}^+ > \tilde{\mu}^-$), positive for the coupled stress-driven formulation (cf. Eq. (105), valid for $\check{\mu}^+ > \check{\mu}^-$ and $\check{\zeta}^+ > 6\check{\mu}^+$), and vanishes for the coupled strain-driven formulation. Furthermore, even if in-plane axial components $\sigma_{xx} = \sigma_{yy} > 0$ for all four cases, note a factor of 4 between respective predictions by the coupled or uncoupled stress-driven formulations.

6.3. Tension-compression response of a plate with a central hole

In the previous examples we have verified numerically that both axial and shear responses computed with ADINA provide exact analytical solutions in uniform deformation states. We simulate here the stretching, under both tension and compression, of a rectangular plate with a concentric circular hole to verify that Eqs. (33) and (37), for strain-driven procedures, as well as Eqs. (40) and (43) along with the local iterations in Eq. (113), for stress-driven procedures, provide respective consistent linearization of stresses for general multi-axial non-uniform deformation states, with different integration points likely presenting different tension-compression states along differently oriented principal directions.

The geometry and finite element discretization are shown in Fig. 9. The plate is stretched $\pm 0.1\%$ (relative to its length) along axis x. We assume perfectly lubricated grips at both ends (free displacements along y) as well as a plane strain condition in direction z (fixed displacements along z at both faces). In this case, we employ fully integrated 27-node brick elements (with $3 \times 3 \times 3$ Gauss integration points), and perform four cyclic tension-compression simulations with respective material constants in Eqs. (119)-(122). Figures 10 to 13 show deformed meshes (magnified) and von Mises stress maps for maximum (0.1%) and minimum (-0.1%) mean axial strain ε_{xx}, which clearly show the existent asymmetric global responses under tension and compression for the four formulations, especially regarding absolute values of stress (respective von Mises maps, under tension and compression, are identical for linear materials). Note that, since all model constants have been determined to give the same uniaxial response (Figure 7) and the in-plane shear stresses predicted by all

four models turned to be very similar (Figure 8), then associated deformed meshes and von Mises stresses also result to be similar, although some differences can be noticed. Nonetheless, higher differences are observed for particular stress components, as one would expect from the results in Figure 8. Finally, similar to what we observed for the tension-compression uniaxial test analyzed above, exact numerical solutions were obtained in a single Newton-Raphson global iteration when no local change of constitutive behavior took place during incremental steps with proportional loading (i.e., for either $\varepsilon_{xx} > 0$ or $\varepsilon_{xx} < 0$ preserved), consistent with a linear computation. For steps involving local changes of constitutive behavior (i.e., for either $\varepsilon_{xx} > 0$ becoming negative or $\varepsilon_{xx} < 0$ becoming positive), additional global iterations were required to obtain a solution, although they showed asymptotically quadratic rates of convergence for both residual force and energy, as shown in Table 2. Indeed, Table 3 shows that convergence (e.g., in the uncoupled strain-driven case) is afforded by progressive iterations with less and less integration points undergoing changes in material switches, with the relevance of the remaining points for which switches are being decided less and less important in the solution (hence in the residual). If there are no changes in the switches, the solution is obtained in just one iteration consistent with a linear problem. Finally, and only for the uncoupled stress-driven formulation with the specific material constants in Eq. (121), global line searches were needed to run a complete tension-compression cyclic test (likely, during initial iterations only, involving resetting of local tangents), with the finite element computation converging quadratically when the globally bi-linear incremental solution was engaged, see Table 2. Noteworthy, other sets of parameters for the uncoupled stress-driven model did not present this numerical issue or need line searches to find an incremental solution during critical, bi-linear, steps.

7. Conclusion

The theory of bi-modulus materials, with different behavior in tension and compression, is applicable to a wide variety of materials. Therefore, departing from the work of Ambartsumyan, several approaches have been presented in the literature to analyse these materials. However, these approaches present a restriction on the elasticity constants (reducing to *three* the independent constants to preserve symmetry and thermodynamic consistency) and result

in complex tangent matrices and corresponding finite element implementations which, frequently, report poor convergence properties, among them a loss of asymptotic second order convergence.

In this work we have presented a generalized framework based on hyperelasticity to deal systematically with this class of materials. We have analysed four possibilities attending to the stress or strain nature of the switches and their coupled or uncoupled setting. In *all* these cases, the presented formulations preserve the expected *four* independent moduli, retaining thermodynamic consistency, symmetry of the constitutive tensors and resulting in simple and efficient finite element formulations. Indeed, the anticipated efficiency for a bilinear material, with at least asymptotic quadratic convergence rates, is obtained as we have shown in the examples.

Acknowledgements

Partial financial support for this work has been given by grant PGC-2018-097257-B-C32 from the Ministerio de Ciencia, Innovación y Universidades of Spain. The ADINA license for the examples has been a courtesy of ADINA R&D to UPM.

Material	$E^+[MPa]$	$E^-[MPa]$	ν^+	ν^-	Refs.
Fine grained Concrete	650	1820	–	–	[21, 26]
Glass fiber KC-30	535	115	–	–	[21, 26]
Glass fiber AC-30	139	20	–	–	[21, 26]
Epoxi E862 resin (at 20^oC)	$2,520$	$2,710$	0.43	0.39	[63]
Epoxi E862 resin (at 80^oC)	$1,950$	$1,660$	0.40	0.37	[63]
Epoxi resin (by Brazilian test)	$1,590 \sim 1,630$	$1,760 \sim 5,590$	–	–	[3]
PLA 3D-printed, filament at 0^o	$3,980$	$4,730$	–	–	[65]
Articular cartilage	12.75	0.60	0.186	0.034	[19]
Georgia marble	$23,400$	$42,100$	–	–	[4, 61]
Russian marble	$9,000$	$20,700$	–	–	[4, 61]
Russian sandstone	$11,700$	$57,200$	–	–	[4, 61]
Granite (different types)	$14,000 \sim 55,200$	$20,000 \sim 68,900$	–	–	[4]
Pinctada nacre	$51,000$	$73,000$	–	–	[6, 62]
Poplar 12%MC (fiber dir.)	$\simeq 8,000$	$\simeq 4,000$	–	–	[57, 58, 66]
Sugar Maple 12%MC (fiber)	$\simeq 12,600$	$\simeq 9,860$	$\simeq 0.45$	$\simeq 0.05$	[58, 60, 64]
Soft traslucent silicone	0.45	0.25	$(\simeq 0.5)$	$(\simeq 0.5)$	[59]
Natural rubber NR70	$3.94 \sim 5.84$	8.33	$(\simeq 0.5)$	$(\simeq 0.5)$	[59]

Table 1: Typical constants for some bimodulus materials

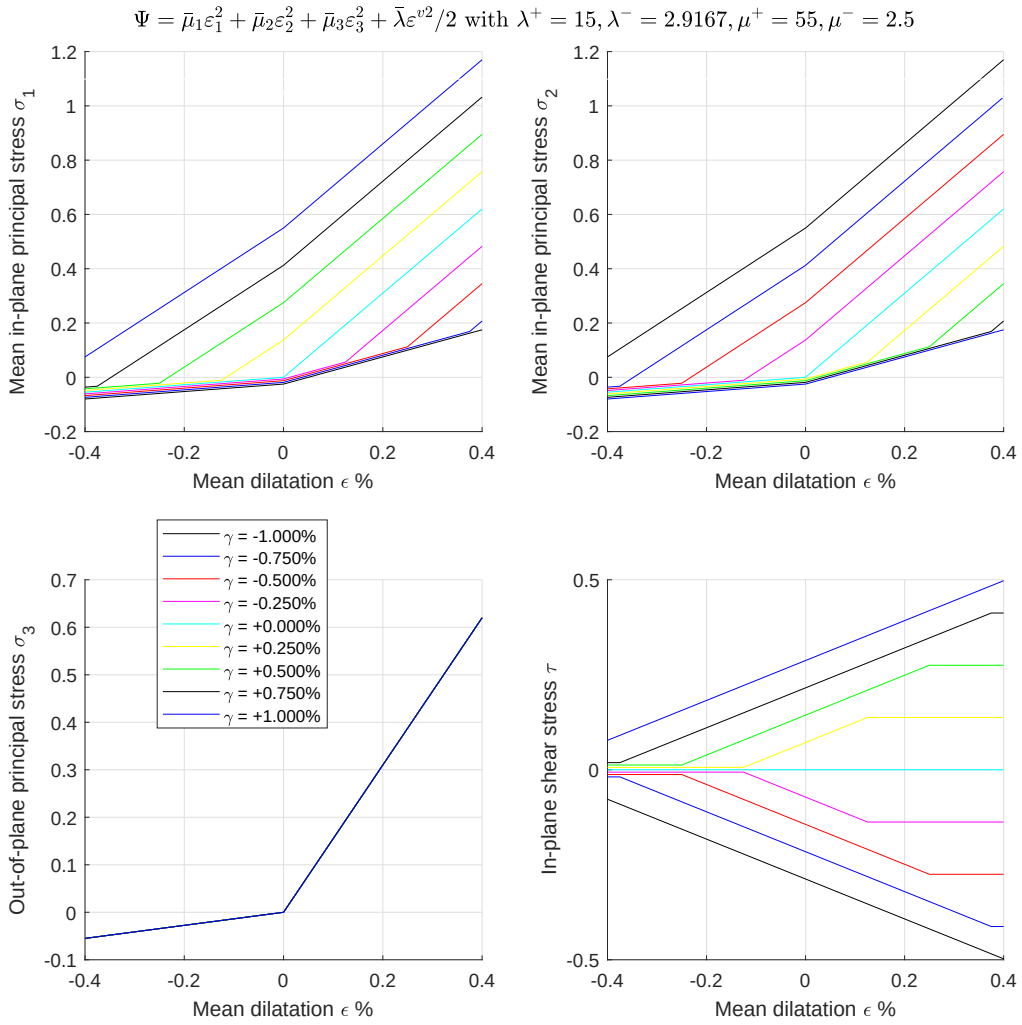

Figure 1: Response of a "bi-modulus" hyperelastic isotropic material employing total strain switches under changes of dilatation and pure shear strain (stress units in [MPa]); principal stresses and in-plane shear stress. Strain energy density function $\Psi(\boldsymbol{\varepsilon}) = \bar{\mu}_1\varepsilon_1^2 + \bar{\mu}_2\varepsilon_2^2 + \bar{\mu}_3\varepsilon_3^2 + \frac{1}{2}\bar{\lambda}\varepsilon^{v2}$.

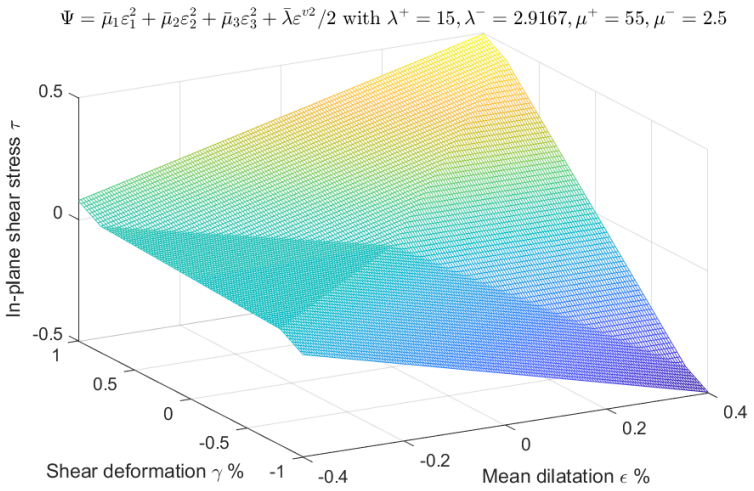

Figure 2: Response of a "bi-modulus" hyperelastic isotropic material employing total strain switches under changes of dilatation and pure shear strain (stress units in [MPa]); shear strain. Strain energy density function $\Psi(\boldsymbol{\varepsilon}) = \bar{\mu}_1\varepsilon_1^2 + \bar{\mu}_2\varepsilon_2^2 + \bar{\mu}_3\varepsilon_3^2 + \frac{1}{2}\bar{\lambda}\varepsilon^{v2}$.

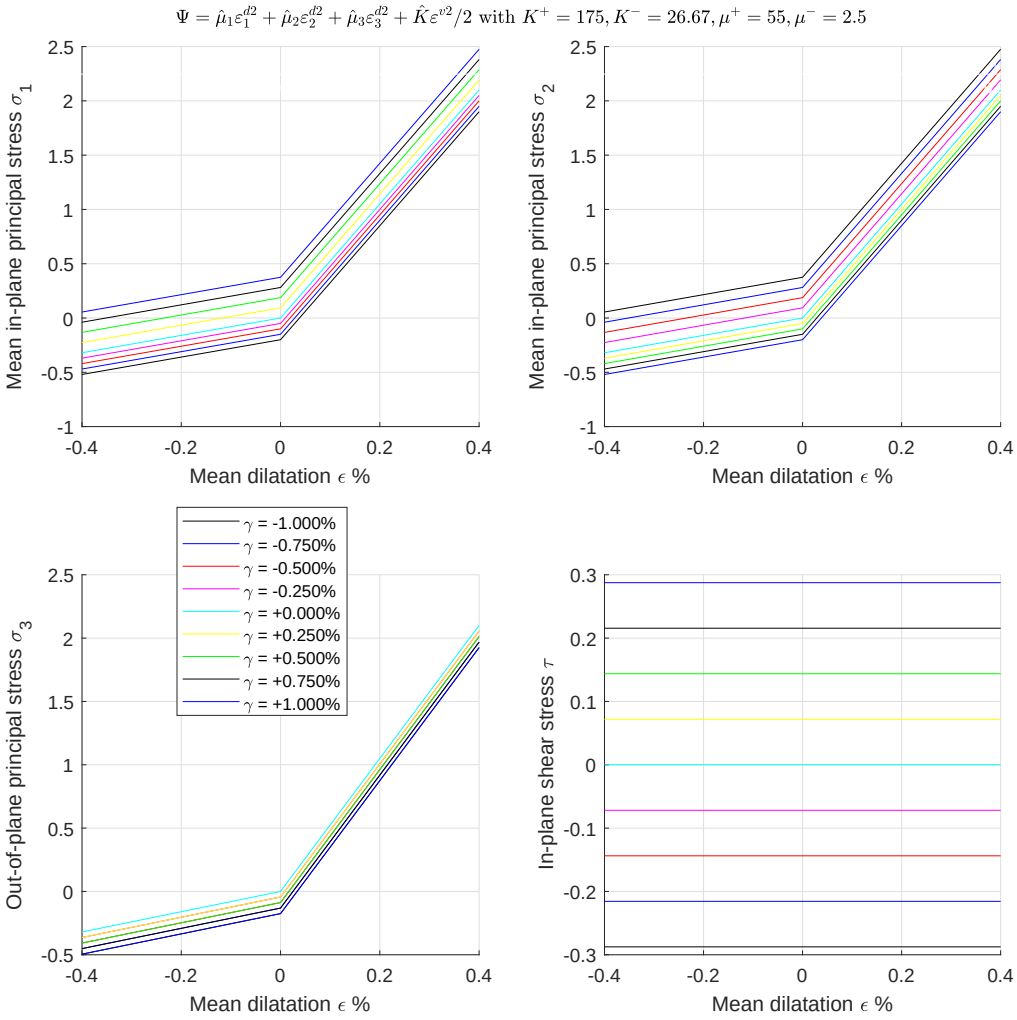

Figure 3: Response of a "bi-modulus" hyperelastic isotropic material employing uncoupled strain switches under changes of dilatation and pure shear strain (stress units in [MPa]); principal stresses and in-plane shear stress. Strain energy density function $\Psi(\boldsymbol{\varepsilon}) = \hat{\mu}_1\varepsilon_1^{d2} + \hat{\mu}_2\varepsilon_2^{d2} + \hat{\mu}_3\varepsilon_3^{d2} + \frac{1}{2}\hat{\lambda}\varepsilon^{v2}$.

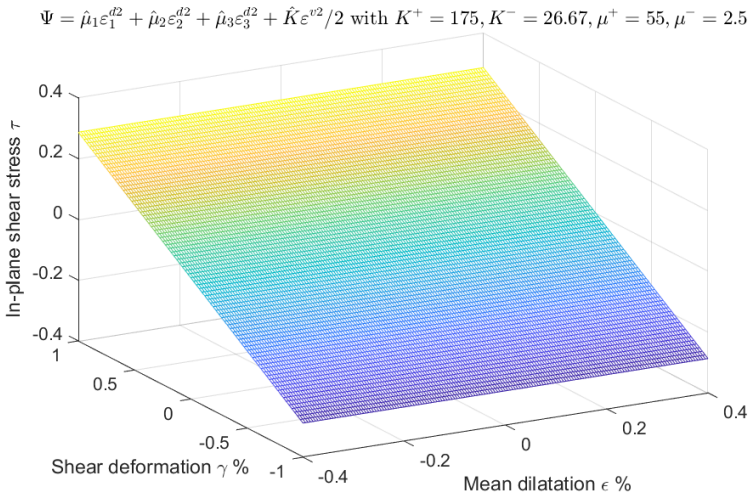

Figure 4: Response of a bi-modulus hyperelastic isotropic material employing uncoupled strain switches under changes of dilatation and pure shear strain (stress units in [MPa]); in-plane shear stress. Strain energy density function $\Psi(\boldsymbol{\varepsilon}) = \bar{\mu}_1 \varepsilon_1^2 + \bar{\mu}_2 \varepsilon_2^2 + \bar{\mu}_3 \varepsilon_3^2 + \frac{1}{2}\bar{\lambda}\varepsilon^{v2}$.

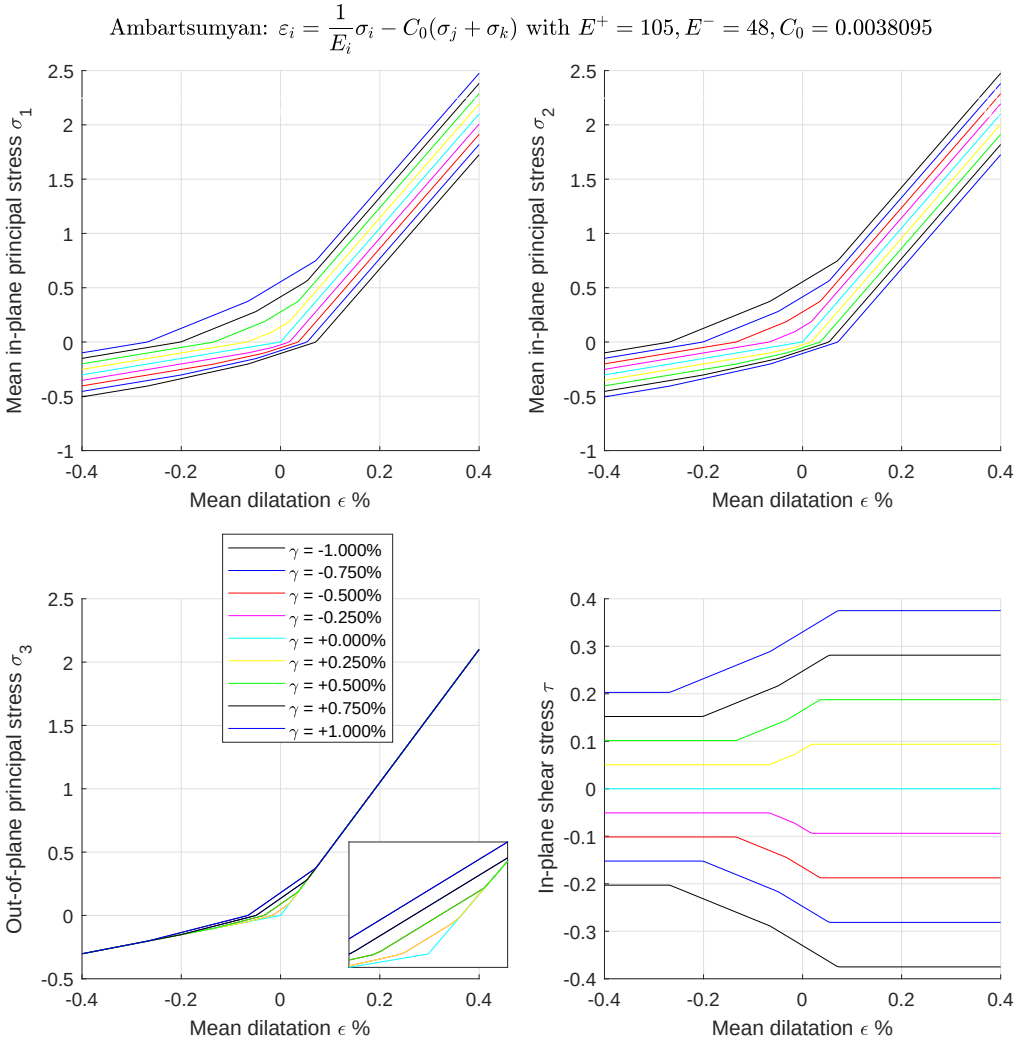

Figure 5: Response of the "bi-modulus" isotropic material from Ambartsumyan employing total stress switches under changes of dilatation and pure shear strain (stress units in [MPa]); principal stresses and in-plane shear stress.

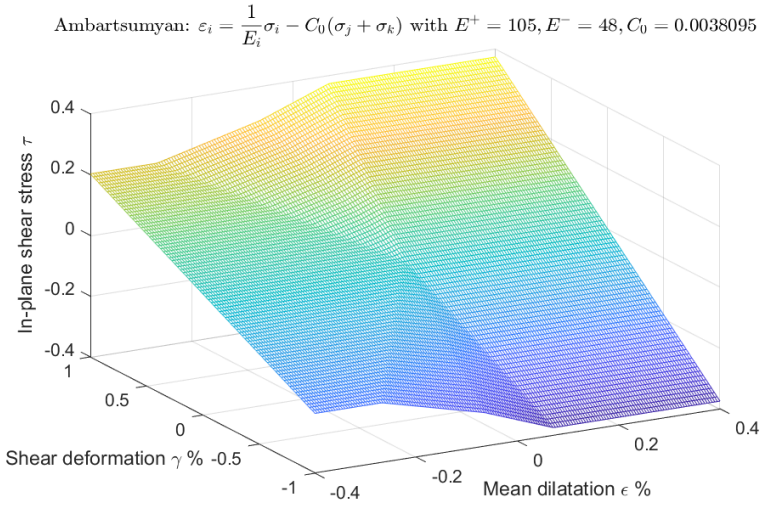

Figure 6: Response of a "bi-modulus" hyperelastic isotropic material employing total strain switches under changes of dilatation and pure shear strain (stress units in [MPa]). Strain energy density function $\Psi(\boldsymbol{\varepsilon}) = \bar{\mu}_1\varepsilon_1^2 + \bar{\mu}_2\varepsilon_2^2 + \bar{\mu}_3\varepsilon_3^2 + \frac{1}{2}\bar{\lambda}\varepsilon^{v2}$.

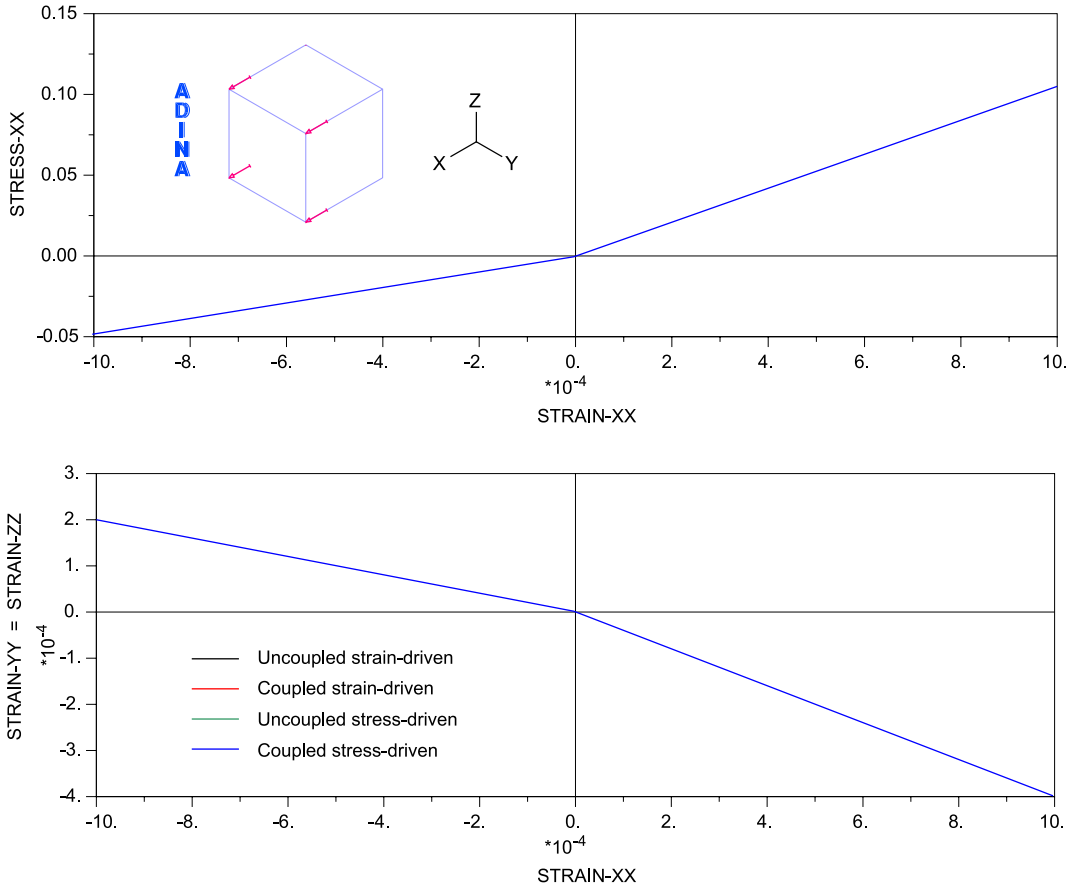

Figure 7: Response curves for uniaxial stress $\sigma_u = \sigma_{xx}$ [MPa] (top panel) and transverse strain $\varepsilon_t = \varepsilon_{yy} = \varepsilon_{zz}$ (bottom panel) as a function of the uniaxial strain $\varepsilon_u = \varepsilon_{xx}$ for four uniaxial test computed with Adina (shown in top panel as well is the single element considered with the axial displacements prescribed) with prescribed uncoupled / coupled or strain / stress based bi-modulus parameters in Eqs. (119)-(122). Note that the experimentally observable Young's bi-modulus and Poisson's bi-ratio in Eq. (118), from which parameters for the four models have been previously determined, are reproduced by respective numerical simulations (with overlapped curves).

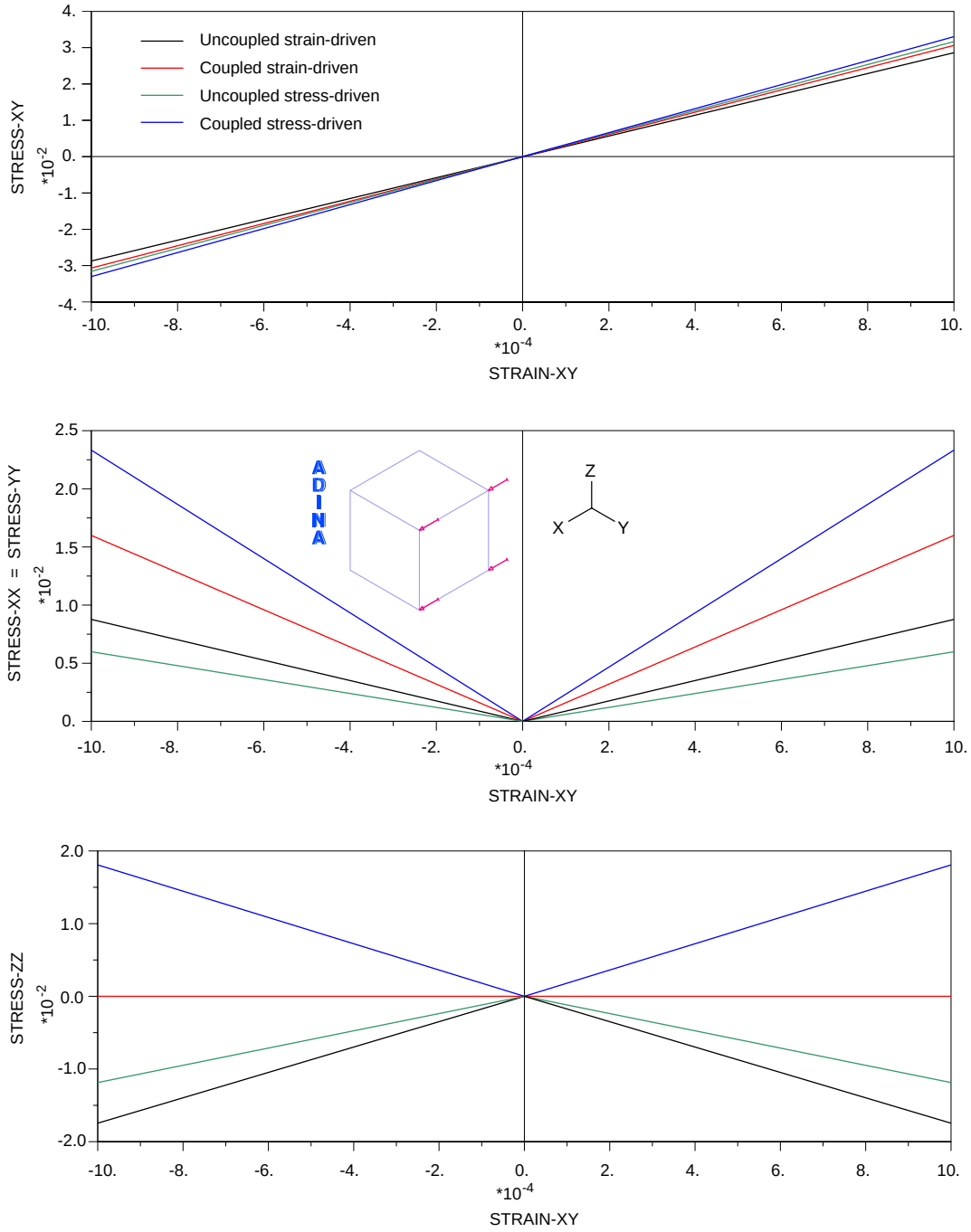

Figure 8: Response curves for shear stress σ_{xy} [MPa] (top panel) as well as axial $\sigma_{xx} = \sigma_{yy}$ (center panel) and σ_{zz} (bottom panel) stress as a function of the shear strain $\gamma_{xy} = 2\varepsilon_{xy}$ for four shear tests computed with Adina (shown in center panel as well is the single element considered with the displacements prescribed) with prescribed uncoupled / coupled or strain / stress based bi-modulus parameters in Eqs. (119)-(122). Note the different responses, especially axial stress components, that different bi-modulus formulations, characterized from a common tension-compression uniaxial test (Figure 7), predict for a shear test.

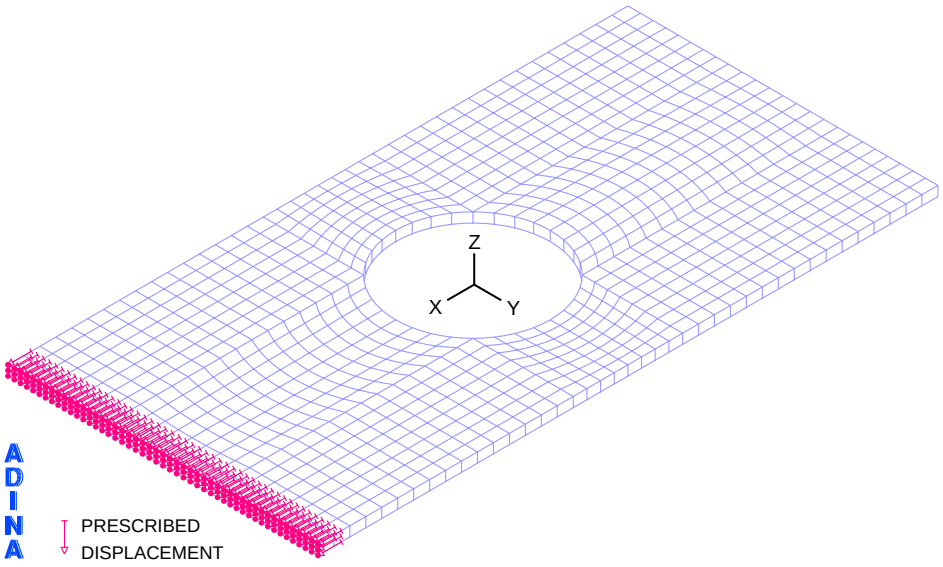

Figure 9: Elongation of a plate with a circular hole under a plane strain condition. Finite element undeformed three-dimensional mesh with applied displacements. Length = 32 mm; Height = 16 mm; Hole Diameter = 8 mm.

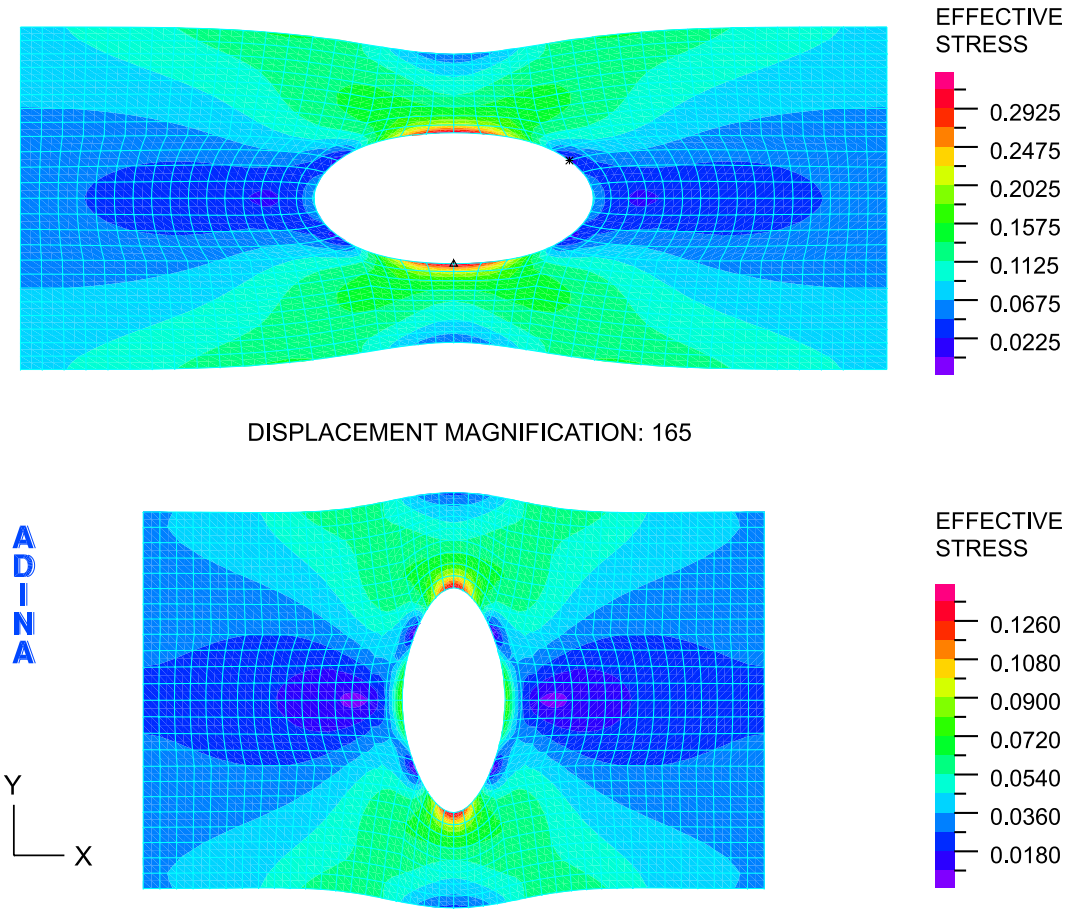

Figure 10: Uncoupled strain-driven formulation: Deformed configurations (magnified by a factor of 165) and non-smoothed band plots of von Mises stress for an overall axial strain $\varepsilon_{xx} = \Delta L_x / L_x = 10^{-3}$ (top) or $\varepsilon_{xx} = \Delta L_x / L_x = -10^{-3}$ (bottom).

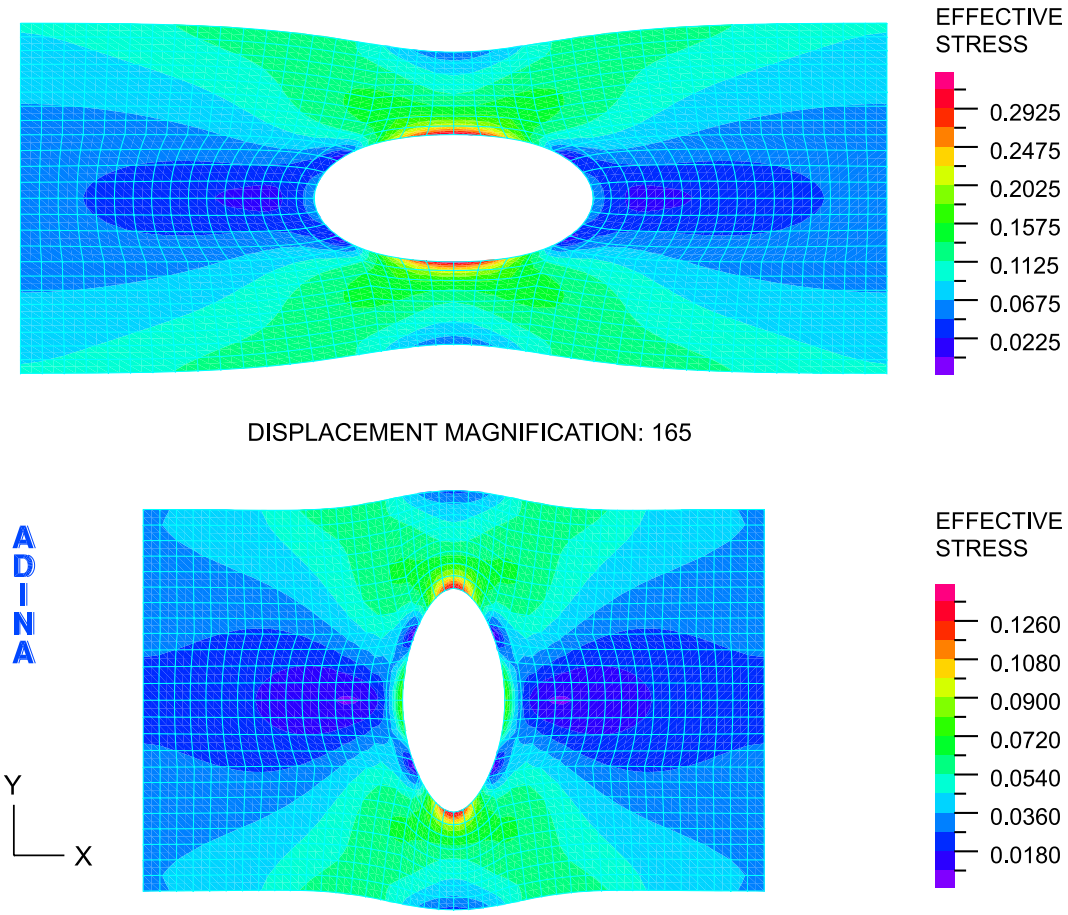

Figure 11: Coupled strain-driven formulation: Deformed configurations (magnified by a factor of 165) and non-smoothed band plots of von Mises stress for an overall axial strain $\varepsilon_{xx} = \Delta L_x/L_x = 10^{-3}$ (top) or $\varepsilon_{xx} = \Delta L_x/L_x = -10^{-3}$ (bottom).

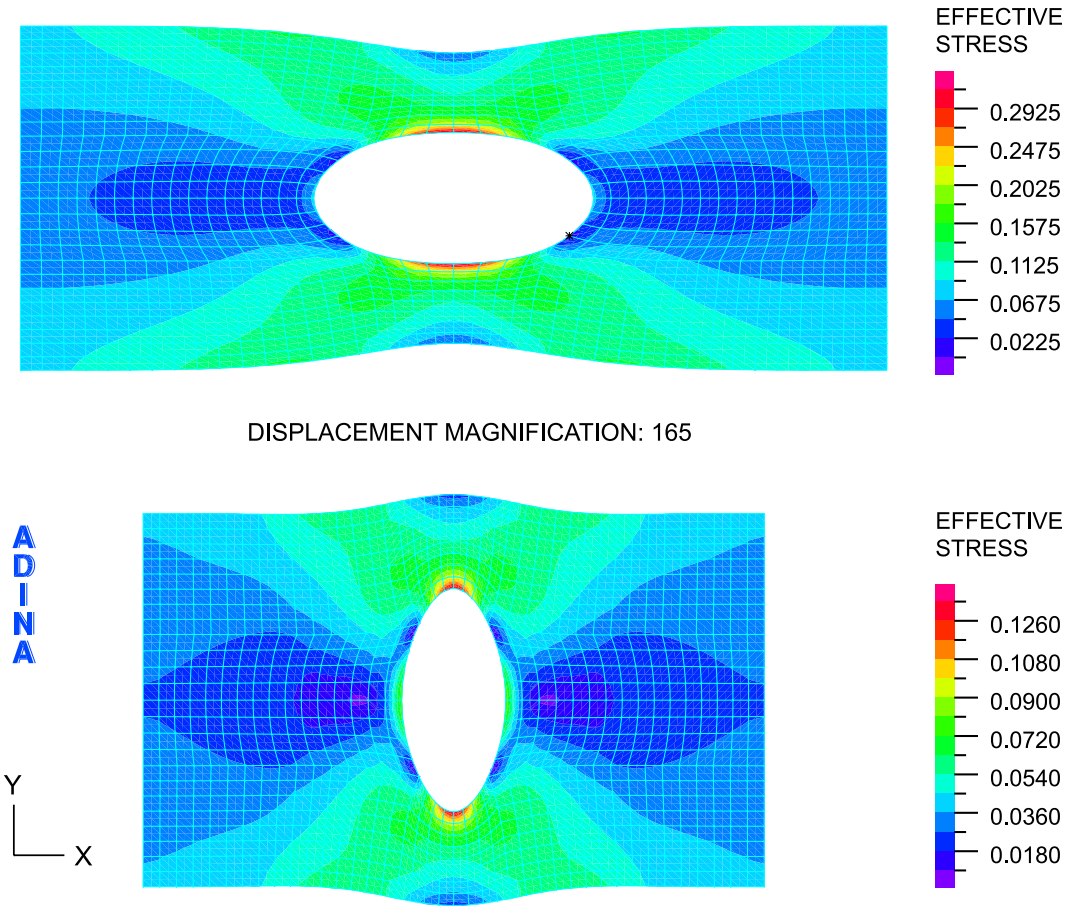

Figure 12: Uncoupled stress-driven formulation: Deformed configurations (magnified by a factor of 165) and non-smoothed band plots of von Mises stress for an overall axial strain $\varepsilon_{xx} = \Delta L_x/L_x = 10^{-3}$ (top) or $\varepsilon_{xx} = \Delta L_x/L_x = -10^{-3}$ (bottom).

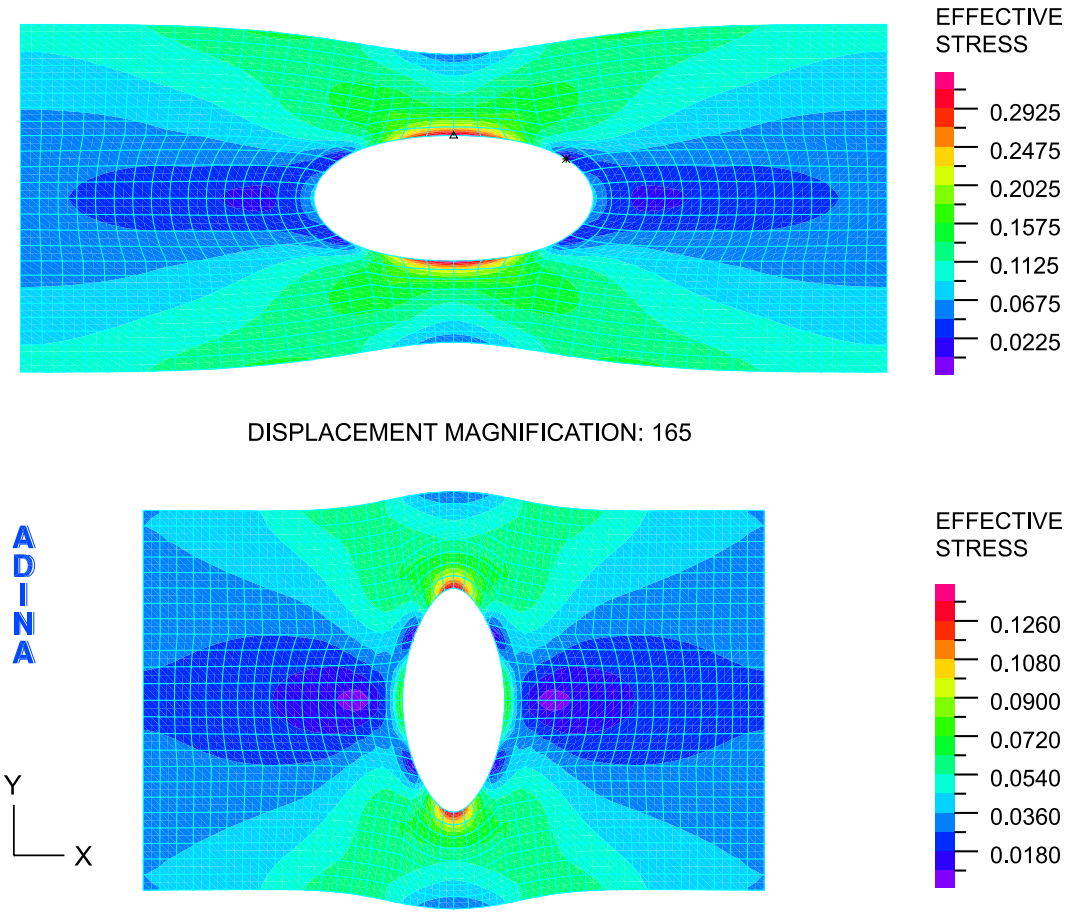

Figure 13: Coupled stress-driven formulation: Deformed configurations (magnified by a factor of 165) and non-smoothed band plots of von Mises stress for an overall axial strain $\varepsilon_{xx} = \Delta L_x/L_x = 10^{-3}$ (top) or $\varepsilon_{xx} = \Delta L_x/L_x = -10^{-3}$ (bottom).

	Uncoupled-Strain		Coupled-Strain		Uncoupled-Stress		Coupled-Stress	
Iter.	Force	Energy	Force	Energy	Force	Energy	Force	Energy
1	6.0E-02	4.8E-04	3.3E-02	3.4E-04	2.1E-01	5.7E-03	3.4E-02	2.0E-04
2	3.9E-03	5.7E-07	2.1E-03	2.7E-07	2.0E-02	1.5E-05	4.1E-03	1.6E-06
3	1.5E-04	2.9E-10	2.9E-05	1.7E-11	4.7E-03	2.4E-07	6.2E-04	2.1E-08
4	5.3E-08	5.2E-17	2.2E-09	8.2E-20	1.7E-04	1.3E-08	5.4E-05	7.5E-11
5	2.1E-14	5.7E-30	6.1E-15	3.9E-31	3.2E-06	1.2E-13	3.7E-09	2.8E-19
6					1.2E-09	3.9E-21	7.2E-15	4.4E-31
7					9.3E-15	5.5E-31		

Table 2: Plate with a hole: residual force (left sub-columns) and energy (right sub-columns) during globally bi-linear elastic incremental steps for the four coupled / uncoupled or strain / stress driven simulations shown in Figs. 10 to 13. Line searches were needed for the uncoupled stress-driven formulation.

	Bi-linear incremental step		Linear incremental step	
Iter.	Deviatoric	Volumetric	Deviatoric	Volumetric
1	11596	12238	0	0
2	2468	409		
3	103	36		
4	18	5		
5	0	0		

Table 3: Plate with a hole; strain-driven uncoupled case (Fig. 10). Number of integration points (out of 24192) for which any shear $\hat{\mu}_i$, $i = 1$, 2, or 3 (left sub-columns) or the bulk $\hat{K}$ (right sub-columns) bi-moduli change their values relative to their respective values in the previous iteration (the first iteration compares values against converged values at the previous load step). Convergence up to machine precision (Table 2) is attained in both globally bi-linear (left) and linear (right) incremental steps with proportional loading at the specific iteration (5 and 1, respectively) for which the complete set of moduli have converged locally throughout the plate.

References

[1] L Zhang, KJ Dong, HT Zhang, B Yan. A 3D PVP co-rotational formulation for large-displacement and small-strain of bi-modulus materials. Finite Elements in Analysis and Design, 2016, 110:20-31.

[2] J Mazars, Y Berthaud, S Ramtani. The unilateral behavior of damaged concrete. Engineering Fracture Mechanics, 1990, 35(4-5):629-635.

[3] JH Ye, FQ Wu, Y Zhang, HG Ji. Estimation of the bi-modulus of materials through deformation measurement in a Brazilian disk test. International Journal of Rock Mechanics & Mining Sciences 2012, 52:122-131.

[4] S Patel, CD Martin. Evaluation of Tensile Young's modulus and Poisson's ratio of a bimodular rock from the displacement measurements in a Brazilian test. Rock Mechanics and Rock Engineering, 2018, 51(2):361-373.

[5] G Liu, R Zhang, Y Yi, L Sun, L Shi, H Jiang, S Ma. Experimental and simulation study on stress concentration of graphite components in tension. Mechanics of Materials, 2019, 130:88-94.

[6] K Bertoldi, D Bigoni, WJ Drugan. Nacre: an orthotropic and bimodular elastic material. Composites Science and Technology, 2008, 68:1363-1375.

[7] AM Hartl, M Jerabek, RW Lang. Anisotropy and compression/tension asymmetry of PP containing soft and hard particles and short glass fibers. EXPRESS Polymer Letters, 2015, 9(7): 658-670.

[8] T Huang, QX Pan, J Jin, JL Zhang, PH Wen. Continuous constitutive model for bi-modulus materials with meshless approach. Applied Mathematical Modelling, 2019, 66:41-58.

[9] M Rohanifar, H Hatami-Marbibi. Numerical modelling of mechanical properties of 2D cellular solids with bi-modulus cell walls. Mechanics of Advanced Materials and Structures, doi: 10.1080/15376494.2018.1563251.

[10] K Gall, H Sehitoglu, YI Chumlyakov, IV Kireeva. Tension-compression asymmetry of the stress-strain response in aged single crystal and polycrystalline NiTi. Acta Materialia, 1999, 47(4):1203-1217.

[11] D Jiang, CM Landis, S Kyriakides. Effects of tension/compression asymmetry on the buckling and recovery of NiTi tubes under axial compression. International Journal of Solids and Structures, 2016, 100:41-53

[12] AN Bucsek, HM Paranjape, AP Stebner. Myths and truths of Nitinol mechanics: elasticity and tension-compression asymmetry. Shape Memory Superelasticity, 2016, 2:264-271.

[13] Y Song, Y Li, W Song, K Yee, KY Lee, VL Tagarielli. Measurements of the mechanical response of unidirectional 3D-printed PLA. Materials and Design, 2017, 123:154-164.

[14] RM Jones. Stress-strain relations for materials with different moduli in tension and compression. AIAA Journal, 1975, 15(1):16-23.

[15] D Bruno, S Lato, E Sacco. Nonlinear analysis of bimodular composite plates under compression. Computational Mechanics, 1994, 14:28-37.

[16] CW Bert. Models for fibrous composites with different properties in tension and compression. Journal of Engineering Materials and Technology–Transactions of the ASME, 1977 (Oct.), 344-349

[17] KM Moerman, CK Simms, T Nagel. Control of tension-compression asymmetry in Ogden hyperelasticity with application to soft tissue modelling. Journal of the Mechanical Behavior of Biomedical Materials, 2016, 56:218-228.

[18] A Mirnajafi, JM Raymer, LR McClure, MS Sacks. The flexural rigidity of the aortic valve leaflet in the commissural leaflet. Journal of Biomechanics, 2006, 39:2966-2973.

[19] MA Soltz, GA Ateshian. A conewise linear elasticity mixture model for the analysis of tension-compression nonlinearity in articular cartilage. Journal of Biomechanical Engineering, 2000, 122:576-587.

[20] M Destrade, MD Gilchrist, JA Motherway, JG Murphy. Bimodular rubber bucles early in bending. Mechanics of Materials, 2010, 42:469-476.

[21] XP Zheng, YP Cao, B Li, XQ Feng, H Jiang, YY Huang. Determining the elastic modulus of thin films using a buckling-based method: computational study. Journal of Physics D: Applied Physics, 2009, 42:175506.

[22] X Huang, B Li, W Hong, YP Cao, XQ Feng. Effects of tension-compression asymmetry on the surface wrinkling of film-substrate systems. Journal of the Mechanics and Physics of Solids, 2016, 94:88-104.

[23] AG Tibert, S Pellegrino. Deployable tensegrity reflectors for small satellites. Journal of Spacecraft and Rockets, 2002, 39(5):701-709.

[24] H Tan, X Du, L Yuyan, Z Gogave, H Baier. Design and development of a large reflector model with inflatable deployment and rib support structures. European Conference on Spacecraft Structures, Metarials and Mechanical Testing, Noordwijk, Netherlands, 10-12 May 2005 (ESA SP-581. August 2005).

[25] DE Ingber. Tensegrity I. Cell structure and hierarchical systems biology. Journal of Cell Science, 2003, 116:1157-1173.

[26] SA Ambartsumyan. Elasticity Theory of Different Moduli (RF Wu, YZ Zhang, Trans.). China Railway Publishing House, Beijing, 1986.

[27] JY Sun, HQ Zhu, SH Qin, DL Yang, XT He. A review on the research of mechanical problems with different moduli in tension and compression. Journal of Mechanical Science and Technology, 2010, 24(9):1845-1854.

[28] H Zhao, Z Ye. Analytic elasticity solution of bi-modulus beams under combined loads. Applied Mathematics and Mechanics–English Ed, 2015, 36(4):427-438.

[29] N Kamiya. An energy method applied to large deflestion of a thin plate of bimodulus material. Journal of Structural Mechanics, 1974, 3(3):317-329.

[30] N Kayima. Transverse shear effect in a bimodulus plate. Nuclear Engineering and Design, 1975, 32(3):351-357.

[31] Z Du, Y Zhang, W Zhang, X Guo. A new computational framework for materials with different mechanical responses in tension and compression and its applications. International Journal of Solids and Structures, 2016, 100-101:54-73.

[32] K Cai, J Cao, J Shi, L Liu, QH Qin. Optimal layout of multiple bi-modulus materials. Structural Multidisciplinary Optimization, 2016, 53:801-811.

[33] K Cai, QH Qin, Z Luo, AJ Zhang. Robust topology optimisation of bi-modulus structures. Computer-Aided Design 2013, 45, 1159-1169.

[34] J Shi, Z Gao. Ill-loaded layout optimization of bi-modulus material. Finnite Elements in Analysis and Design, 2015, 95:51-61.

[35] Z Du, W Zhang, Y Zhang, R Xue, X Guo. Structural topology optimization involving bi-modulus materials with asymmetric properties in tension and compression. Computational Mechanics, 2018, 10.1007/s00466-018-1597-2.

[36] R Chunjiang, Y Haitian, Z Guoqing. A gradient based algorithm to solve inverse plane bimodular problems of identification. Journal of Computational Physics, 2018, 355:78-94.

[37] G Medri. A nonlinear elastic model for isotropic materials with different behavior in tension and compression. Journal of Engineering Materials and Technology–Transactions of the ASME, 1982, 104:26-28.

[38] K Vijayakumar, KP Rao. Stress-strain relations for composites with different stiffnesses in tension and compression. A new material model. Computational Mechanics, 1987, 2:167-175.

[39] HW Zhang, L Zhang, Q Gao. An efficient computational method for mechanical analysis of bimodular structures based on parametric variational principle. Computers and Structures, 2011, 89:2352-2360.

[40] Z Du, X Guo. Variational principles and the related bounding theorems for bi-modulus materials. Journal of the Mechanics and Physics of Solids, 2014, 73:183-211.

[41] Z Rigbi. Some thoughts concerning the existence or otherwise of an isotropic bimodulus material. Journal of the Engineering Materials and Technology–Transactions of the ASME, 1980, 102:383-384.

[42] XT He, ZL Zheng, JY Sun, YM Li, SL Chen. Convergence analysis of a finite element method based on different moduli in tension and compression. International Journal of Solids and Structures, 2009, 46(20):3734-3740.

[43] J Crespo, M Latorre, FJ Montáns. WYPIWYG hyperelasticity for isotropic, compressible materials. Computational Mechanics, 2017, 59(1):73-92.

[44] M Latorre, M Melika and CK Simms, FJ Montáns. A continuum model for tension-compression asymmetry in skeletal muscle. Journal of the mechanical behavior of biomedical materials, 2018, 77:455-460.

[45] M Latorre, FJ Montáns. Stress and strain mapping tensors and general work-conjugacy in large strain continuum mechanics. Applied Mathematical Modelling, 2016, 40(5):3938-3950.

[46] KJ Bathe. Finite element procedures. Second Edition, Watertown: KJ Bathe, 2014.

[47] M Latorre, FJ Montáns. On the interpretation of the logarithmic strain tensor in an arbitrary system of representation. International Journal of Solids and Structures, 2014, 51(7-8):1507-1515.

[48] M Kojic, KJ Bathe. Inelastic Analysis of Solids and Structures. Springer, Berlin, 2005.

[49] MA Caminero, FJ Montáns, KJ Bathe. Modeling large strain anisotropic elasto-plasticity with logarithmic strain and stress measures. Computers and Structures, 2011; 89(11-12): 826-843.

[50] M Latorre, FJ Montáns. A new class of plastic flow evolution equations for anisotropic multiplicative elastoplasticity based on the notion of a corrector elastic strain rate. Applied Mathematical Modelling, 2018, 55:716-740.

[51] M Latorre, FJ Montáns, M Latorre. Computational anisotropic hardening multiplicative elastoplasticity based on the corrector elastic logarithmic strain rate. Computer Methods in Applied Mechanics and Engineering, 2017, 320:82-121.

[52] M Latorre, FJ Montáns. Fully anisotropic finite strain viscoelasticity based on a reverse multiplicative decomposition and logarithmic strains. Computers and Structures, 2016, 99:57-70.

[53] M Latorre, FJ Montáns. What-You-Prescribe-Is-What-You-Get orthotropic hyperelasticity. Computational Mechanics, 2014, 53(6):1279-1298.

[54] M Latorre, X Romero, FJ Montáns. The relevance of transverse deformation effects in modeling soft biological tissues. International Journal of Solids and Structures, 2016, 99:57-70.

[55] M Latorre, FJ Montáns. Material symmetries congruency in transversely isotropic and orthotropic hyperelastic materials. European Journal of Mechanics-A/Solids, 2015, 53:99-106.

[56] ADINA, Theory and Modelling Guide, ADINA R&D, Watertown, 2012 ARD 12-8.

[57] M Casado, L Acuna, D Vecilla, E Relea, A Basterra, G Ramon, G Lopez (2010). The influence of size in predicting the elastic modulus of Populus x Americana timber using vibration techniques. In: Structures and Architecture, Cruz (Ed.), Taylor & Francis, London, 2025-2032.

[58] TE Conners, PJ Medvecz. Wood as a bimodular material. Wood and Fiber Science, 1992, 24(4):413-423.

[59] M Destrade, JG Murphy, B Rashid. Differences in tension and compression in the nonlinearly elastic bending of beams. International Journals of Structural Changes in Solids, 2009, 1:29-37.

[60] DW Green, JE Winandy, DE Kretschmann. Ch 3: Mechanical properties of wood. In: Wood handbook—Wood as an engineering material, Rep. FPL-GTR-113. U.S. Department of Agriculture, Forest Service, Forest Products Laboratory, Madison.

[61] BC Haimson, TM Tharp. Stress around boreholes in bilinear elastic rock. Journal of the Society of Petroleum Engineering, 1974, 14(2):145-151

[62] AP Jackson, JFV Vicent, RM Turner. The mechanical design of nacre. Proceedings of the Royal Society of London, 1988, 234:415-440.

[63] JD Littell, CR Ruggeri, RK Goldberg, GD Roberts, WA Arnold, WK Binienda. Measurement of epoxy resin tension, compression, and shear stress-strain curves over a wide range of strain rates using small test specimens. Journal of Aerospace Engineering, ASCE, 2008, 21:162-173.

[64] MH Schenider, DA Phillips, DA Tingley, KI Brebner. Mechanical properties of polymer-impregnated sugar maple. Forest Production Journal, 1990, 40(1):37-41

[65] Y Song, Y Li, W Song, K Yee, K-Y Lee, VL Tagarielli. Measurements of the mechanical response of unidirectional 3D-printed PLA. Materials and Design, 2017, 123:154-164.

[66] BD Zakic. Stress distribution within the plastic range in wood beam subjected to pure bending. Holzforschung und Holzerwertung, 1976, 28(5):114-120

[67] L Zhang, H Zhang, J Wu, B Yan, M Lu. Parametric variational principle for bi-modulus materials and its application to Nacreous bio-composites. International Journal of Applied Mechanics, 2016, 8(6):1650082.